Set-valued state estimation of nonlinear discrete-time systems with nonlinear invariants based on constrained zonotopes☆

Brenner S. Rego [a,*], Joseph K. Scott [b], Davide M. Raimondo [c], Guilherme V. Raffo [a,d]

[a] Graduate Program in Electrical Engineering, Federal University of Minas Gerais, Belo Horizonte, MG 31270-901, Brazil
[b] Department of Chemical and Biomolecular Engineering, Georgia Institute of Technology, Atlanta, GA, USA
[c] Department of Electrical, Computer and Biomedical Engineering, University of Pavia, Italy
[d] Department of Electronics Engineering, Federal University of Minas Gerais, Belo Horizonte, MG 31270-901, Brazil

ARTICLE INFO

Keywords:
Nonlinear state estimation
Nonlinear state constraints
Set-based computing
Constrained zonotopes

ABSTRACT

This paper presents new methods for set-valued state estimation of discrete-time nonlinear systems whose trajectories are known to satisfy nonlinear equality constraints, called *invariants* (e.g., conservation laws). Set-valued estimation aims to compute tight enclosures of the possible system states in each time step subject to unknown-but-bounded uncertainties. Most existing methods employ a standard prediction-update framework with set-based prediction and update steps based on various set representations and techniques. However, achieving accurate enclosures for nonlinear systems remains a significant challenge. This paper presents new methods based on constrained zonotopes that improve the standard prediction-update framework for systems with invariants by adding a *consistency step*. This new step uses invariants to reduce conservatism and is enabled by new algorithms for refining constrained zonotopes based on nonlinear constraints. This paper also presents significant improvements to existing prediction and update steps for constrained zonotopes. Specifically, new update algorithms are developed that allow nonlinear measurement equations for the first time, and existing prediction methods based on conservative approximation techniques are modified to allow a more flexible choice of the approximation point, which can lead to tighter enclosures. Numerical results demonstrate that the resulting methods can provide significantly tighter enclosures than existing zonotope-based methods while maintaining comparable efficiency.

1. Introduction

In recent decades, the importance of state estimation has gained attention in many fields of research (Simon, 2006). This includes a wide range of applications such as state-feedback control (Goodarzi & Lee, 2017; Jaulin, 2009; Rego & Raffo, 2019), fault detection and isolation (Combastel, 2015; Raimondo et al., 2016; Zhang & Jiang, 2008), and robot localization (Saeedi et al., 2016). In contrast to Bayesian strategies such as Kalman filtering (Simon, 2010; Teixeira et al., 2009), set-valued state estimation methods aim to provide guaranteed enclosures of the system trajectories in applications affected by unknown-but-bounded uncertainties, without assuming knowledge of their stochastic properties (Chisci et al., 1996; Schweppe, 1968). To date, most studies on set-valued state estimation have addressed linear systems (Chabane et al., 2014; Girard & Guernic, 2008; Le et al., 2013; Scott et al., 2016), and accurate set-valued estimation of nonlinear systems remains a significant challenge (Alamo et al., 2005; Jaulin, 2016; Rego et al., 2020).

Even for linear discrete-time systems, the exact set of states consistent with the system model and measurements up to a given time k can become arbitrarily complex as k increases. Therefore, to avoid a dramatic increase in computational time (Shamma & Tu, 1997), set-based estimation methods must enclose these sets with simpler set representations of limited complexity, such as intervals (Jaulin, 2009, 2016; Rego et al., 2018b; Yang & Scott, 2020), ellipsoids (Durieu et al., 2001; Polyak et al., 2004), parallelotopes (Chisci et al., 1996), or zonotopes (Alamo et al., 2005, 2008; Combastel, 2005). Unfortunately, for nonlinear systems of practical complexity, such enclosures often become very conservative. There are multiple reasons for this, including the inability of the set representation to capture key features of the sets of interest (e.g., nonconvexity and asymmetry), challenges associated with propagating sets through nonlinear dynamics (e.g., the dependency problem, the wrapping effect,

☆ The material in this paper was not presented at any conference. This paper was recommended for publication in revised form by Associate Editor Andrea Garulli under the direction of Editor Torsten Söderström.

* Corresponding author.
E-mail addresses: brennersr7@ufmg.br (B.S. Rego), joseph.scott@chbe.gatech.edu (J.K. Scott), davide.raimondo@unipv.it (D.M. Raimondo), raffo@ufmg.br (G.V. Raffo).

conservative linearization errors, etc.), and challenges associated with refining sets based on new measurements (e.g., the fact that intersections cannot be enclosed both accurately and efficiently for any of the sets mentioned above save intervals). As a consequence, existing set-based state estimation algorithms have only been applied to relatively simple nonlinear models, and most methods assume linear measurement equations (Combastel, 2005; Rego et al., 2020, 2018b) although the measurements available in many practical examples are nonlinear (Rego et al., 2018a; Teixeira et al., 2009).

In this paper, we present new set-based state estimation algorithms with improved accuracy for the specific case of nonlinear systems whose solutions satisfy a set of potentially nonlinear equality constraints, referred to as *invariants*. The trajectories of such systems evolve on a lower-dimensional manifold embedded in the state space. This is true for many systems of practical interest, including models of (bio)chemical reaction networks (Shen & Scott, 2017), attitude estimation in aircraft systems (Goodarzi & Lee, 2017), and the pose of the body frame in humanoids (Rotella et al., 2014). In the stochastic state estimation framework, invariants have previously been used to force the estimated states to lie on the embedded manifold (Eras-Herrera et al., 2019; Julier & LaViola, 2010; Simon, 2010; Teixeira et al., 2009; Yang & Blash, 2009). In the set-based estimation framework considered here, the aim is to use invariants to reduce the conservatism of the enclosure computed in each time step by eliminating enclosed regions that can be proven to violate the invariants, and hence cannot contain real trajectories. Such refinement is known to be very effective at reducing conservatism in interval-based nonlinear reachability calculations (Scott et al., 2013; Shen & Scott, 2017; Yang & Scott, 2020). To the best of the authors' knowledge, the only prior studies that have used invariants in set-based state estimation are Yang and Li (2009) and Yang and Scott (2018a). In Yang and Li (2009), the authors propose a set-valued state estimator using ellipsoids. A linear matrix inequality approach is used to design the estimator taking into account the nonlinear state equality constraints. However, the method only applies to linear dynamics, and the nonlinear state constraints must be conservatively linearized. Moreover, an effective procedure for computing rigorous and accurate linearization error bounds is not provided. In Yang and Scott (2018a), the authors propose an effective method for using invariants to reduce the conservatism of a set-based state estimation method based on differential inequalities and interval analysis. However, the method is limited to systems that have been discretized by Euler approximation with a sufficiently small step size, which can be restrictive in some cases. Moreover, although the theory is general, the provided algorithm only applies to linear invariants and linear measurement equations.

This paper proposes two new methods for set-valued state estimation of discrete-time nonlinear systems with nonlinear measurements and invariants. These algorithms represent enclosures using constrained zonotopes (Scott et al., 2016) and are based on two different methods for propagating these enclosures through nonlinear mappings called the mean value extension and first-order Taylor extension, respectively. Both algorithms are based on the standard prediction-update framework used in most existing approaches in which an enclosure of the system states at time k is first propagated through the dynamics to obtain an enclosure of the possible states at time $k+1$ (prediction), and this enclosure is subsequently refined based on the new measurement at $k+1$ (update). We generalize both the mean value and first-order Taylor-based prediction-update algorithms recently proposed in Rego et al. (2020), which are based on conservative approximation techniques. These generalizations allow for a more flexible choice of the approximation point used in the prediction step and also enable new update algorithms applicable to nonlinear measurement equations, which were not considered in Rego et al. (2020). Furthermore, we add a new step to this framework, referred to as the *consistency step*, which further refines the enclosure at $k+1$ using the nonlinear invariants, leading to improved accuracy. The new nonlinear update and consistency steps are specifically enabled by new mean value and first-order Taylor-based algorithms for effectively refining a constrained zonotope based on nonlinear constraints. Finally, we provide numerical results demonstrating that the proposed methods can provide significantly tighter enclosures than existing zonotope-based methods for systems with invariants while maintaining comparable efficiency.

The remainder of the manuscript is organized as follows. The set-based state estimation problem and the class of nonlinear systems considered are described in Section 2. Section 3 presents mathematical background on constrained zonotopes and other topics. The main results are given in Section 4, including the new consistency and update algorithms and the improvements of the prediction algorithms from Rego et al. (2020). Numerical examples are presented in Section 5, and Section 6 concludes the manuscript.

2. Problem formulation

Let $\mathbf{f}:\mathbb{R}^n\times\mathbb{R}^{n_u}\times\mathbb{R}^{n_w}\to\mathbb{R}^n$ and $\mathbf{g}:\mathbb{R}^n\times\mathbb{R}^{n_u}\times\mathbb{R}^{n_v}\to\mathbb{R}^{n_y}$ be of class $\mathcal{C}^2$ and consider the nonlinear discrete-time system

$$\begin{aligned}\mathbf{x}_k &= \mathbf{f}(\mathbf{x}_{k-1},\mathbf{u}_{k-1},\mathbf{w}_{k-1}), && k\geq 1,\\ \mathbf{y}_k &= \mathbf{g}(\mathbf{x}_k,\mathbf{u}_k,\mathbf{v}_k), && k\geq 0,\end{aligned} \tag{1}$$

where $\mathbf{x}_k\in\mathbb{R}^n$ denotes the system state, $\mathbf{u}_k\in\mathbb{R}^{n_u}$ is the known input, $\mathbf{w}_k\in\mathbb{R}^{n_w}$ is the process uncertainty, $\mathbf{y}_k\in\mathbb{R}^{n_y}$ is the measured output, and $\mathbf{v}_k\in\mathbb{R}^{n_v}$ is the measurement uncertainty. The initial condition and uncertainties are assumed to be unknown-but-bounded, i.e., $\mathbf{x}_0\in\bar{X}_0$, $\mathbf{w}_k\in W$, and $\mathbf{v}_k\in V$, where $\bar{X}_0$, W, and V are known polytopic sets.

This paper presents an improved set-valued state estimation method for systems satisfying known invariants, as defined in the following assumption.

Assumption 1. There exists a $\mathcal{C}^2$ function $\mathbf{h}:\mathbb{R}^n\to\mathbb{R}^{n_h}$ such that, for every solution of (1) with $\mathbf{x}_0\in\bar{X}_0$, $\mathbf{w}_k\in W$, and $\mathbf{v}_k\in V$,

$$\mathbf{h}(\mathbf{x}_0)=\mathbf{0} \quad\Longrightarrow\quad \mathbf{h}(\mathbf{x}_k)=\mathbf{0},\quad \forall k\geq 0. \tag{2}$$

We refer to the elements of $\mathbf{h}$ as *invariants*.

Remark 1. A sufficient condition for (2) is that $\mathbf{h}(\mathbf{f}(\mathbf{x}_k,\mathbf{u}_k,\mathbf{w}_k))=\mathbf{0}$ for all $\mathbf{x}_k$ such that $\mathbf{h}(\mathbf{x}_k)=\mathbf{0}$, for all $\mathbf{w}_k\in W$, and $\mathbf{u}_k$ with $k\geq 0$.

Many systems of practical interest obey invariants describing, e.g., material conservation laws in chemical systems, conservation of energy or momentum in mechanical systems, or the isometry inherent to orientation dynamics in aerospace and robotic systems (Goodarzi & Lee, 2017; Rotella et al., 2014; Shen & Scott, 2017). Prior work on nonlinear reachability analysis has shown that, if used properly, even simple physical information in the form of invariants can dramatically improve the accuracy of reachability bounds computed by interval methods (Scott et al., 2013; Shen & Scott, 2017; Yang & Scott, 2020). Similarly, our aim here is to develop new algorithms for effectively using invariants to improve the accuracy of the state-of-the-art state estimation algorithms based on constrained zonotopes from Rego et al. (2020).

For any $k\geq 0$, let X_k denote the set of all states $\mathbf{x}_k$ that are consistent with (i) the nonlinear model (1), (ii) the measured

output sequence up to time k, $(\mathbf{y}_0, \ldots, \mathbf{y}_k)$, and (iii) the unknown-but-bounded uncertainties $\mathbf{x}_0 \in \{\mathbf{x} \in \bar{X}_0 : \mathbf{h}(\mathbf{x}) = \mathbf{0}\}$, $\mathbf{w}_k \in W$, and $\mathbf{v}_k \in W$, $\forall k \geq 0$. Since exact characterization of X_k is generally intractable (Kühn, 1998; Platzer & Clarke, 2007), the objective of set-valued state estimation is to approximate X_k as accurately as possible by a guaranteed enclosure $\tilde{X}_k \supseteq X_k$. We accomplish this here by extending the standard prediction-update estimation framework with a new consistency step for tightening the enclosures using invariants. The general scheme is given by the following recursion:

$$\bar{X}_k \supseteq \{\mathbf{f}(\mathbf{x}_{k-1}, \mathbf{u}_{k-1}, \mathbf{w}_{k-1}) : \mathbf{x}_{k-1} \in \tilde{X}_{k-1},\ \mathbf{w}_{k-1} \in W\}, \tag{3}$$

$$\hat{X}_k \supseteq \{\mathbf{x}_k \in \bar{X}_k : \mathbf{g}(\mathbf{x}_k, \mathbf{u}_k, \mathbf{v}_k) = \mathbf{y}_k,\ \mathbf{v}_k \in V\}, \tag{4}$$

$$\tilde{X}_k \supseteq \{\mathbf{x}_k \in \hat{X}_k : \mathbf{h}(\mathbf{x}_k) = \mathbf{0}\}, \tag{5}$$

where (3) is the *prediction step*, (4) is the *update step*, (5) is the *consistency step*, and the scheme is initialized with $\bar{X}_0$ in the update step. According to the definition of X_k, we have that $X_0 = \{\mathbf{x}_0 \in \bar{X}_0 : \mathbf{h}(\mathbf{x}_0) = \mathbf{0},\ \mathbf{g}(\mathbf{x}_0, \mathbf{u}_0, \mathbf{v}_0) = \mathbf{y}_0,\ \mathbf{v}_0 \in V\}$. This immediately implies that $\tilde{X}_0 \supseteq X_0$. If $\tilde{X}_{k-1}$ is a valid enclosure of X_{k-1} for some $k \geq 1$, then standard results in set-valued state estimation show that $\hat{X}_k \supseteq X_k$ (Chisci et al., 1996; Le et al., 2013). Since any $\mathbf{x}_{k-1} \in X_{k-1}$ emanates from some $\mathbf{x}_0 \in \bar{X}_0$ satisfying $\mathbf{h}(\mathbf{x}_0) = \mathbf{0}$ by definition, Assumption 1 implies that $\mathbf{h}(\mathbf{x}_k) = \mathbf{0}$, and it follows that $\tilde{X}_k \supseteq X_k$ as well. By induction, we conclude that $\tilde{X}_k \supseteq X_k$ for all $k \geq 0$ as desired.

In the remainder of the paper, our goal is to develop methods for computing accurate enclosures for each of the three steps (3)–(5). Building on prior results in Rego et al. (2020), the main results include generalizations of the prediction methods in Rego et al. (2020) with improved accuracy, new update methods that are applicable to nonlinear measurement equations, and methods for the new consistency step to make effective use of invariants.

3. Preliminaries

The methods in this article use constrained zonotopes, which are an extension of zonotopes proposed in Scott et al. (2016) capable of describing asymmetric convex polytopes, while maintaining many of the well-known computational benefits of zonotopes.

Definition 1. A set $Z \subset \mathbb{R}^n$ is a *constrained zonotope* if there exists $(\mathbf{G}_z, \mathbf{c}_z, \mathbf{A}_z, \mathbf{b}_z) \in \mathbb{R}^{n \times n_g} \times \mathbb{R}^n \times \mathbb{R}^{n_c \times n_g} \times \mathbb{R}^{n_c}$ such that

$$Z = \{\mathbf{c}_z + \mathbf{G}_z\boldsymbol{\xi} : \|\boldsymbol{\xi}\|_\infty \leq 1, \mathbf{A}_z\boldsymbol{\xi} = \mathbf{b}_z\}. \tag{6}$$

We refer to (6) as the *constrained generator representation* (CG-rep). Each column of $\mathbf{G}_z$ is a *generator*, $\mathbf{c}_z$ is the *center*, and $\mathbf{A}_z\boldsymbol{\xi} = \mathbf{b}_z$ are the *constraints*. We use the shorthand notation $Z = \{\mathbf{G}_z, \mathbf{c}_z, \mathbf{A}_z, \mathbf{b}_z\}$. Similarly, we denote standard zonotopes by $Z = \{\mathbf{G}_z, \mathbf{c}_z\} \triangleq \{\mathbf{c}_z + \mathbf{G}_z\boldsymbol{\xi} : \|\boldsymbol{\xi}\|_\infty \leq 1\}$. In addition, we denote by $B_\infty(\mathbf{A}_z, \mathbf{b}_z) \triangleq \{\boldsymbol{\xi} \in \mathbb{R}^{n_g} : \|\boldsymbol{\xi}\|_\infty \leq 1,\ \mathbf{A}_z\boldsymbol{\xi} = \mathbf{b}_z\}$ and $B_\infty^{n_g} \triangleq \{\boldsymbol{\xi} \in \mathbb{R}^{n_g} : \|\boldsymbol{\xi}\|_\infty \leq 1\}$, respectively, the n_g-dimensional constrained and unconstrained unitary hypercubes[1].

Let $Z, W \subset \mathbb{R}^n$, $\mathbf{R} \in \mathbb{R}^{m \times n}$, and $Y \subset \mathbb{R}^m$. Define the linear mapping, Minkowski sum, and generalized intersection as

$$\mathbf{R}Z \triangleq \{\mathbf{R}\mathbf{z} : \mathbf{z} \in Z\}, \tag{7}$$

$$Z \oplus W \triangleq \{\mathbf{z} + \mathbf{w} : \mathbf{z} \in Z,\ \mathbf{w} \in W\}, \tag{8}$$

$$Z \cap_{\mathbf{R}} Y \triangleq \{\mathbf{z} \in Z : \mathbf{R}\mathbf{z} \in Y\}. \tag{9}$$

With these definitions, $Z = \{\mathbf{G}_z, \mathbf{c}_z, \mathbf{A}_z, \mathbf{b}_z\}$ can be viewed as an affine transformation of $B_\infty(\mathbf{A}_z, \mathbf{b}_z)$, $Z = \mathbf{c}_z \oplus \mathbf{G}_z B_\infty(\mathbf{A}_z, \mathbf{b}_z)$. Given W and Y also in CG-rep, the results of the operations (7)–(9) are given in CG-rep as

$$\mathbf{R}Z = \{\mathbf{R}\mathbf{G}_z, \mathbf{R}\mathbf{c}_z, \mathbf{A}_z, \mathbf{b}_z\}, \tag{10}$$

$$Z \oplus W = \left\{\begin{bmatrix}\mathbf{G}_z & \mathbf{G}_w\end{bmatrix}, \mathbf{c}_z + \mathbf{c}_w, \begin{bmatrix}\mathbf{A}_z & \mathbf{0} \\ \mathbf{0} & \mathbf{A}_w\end{bmatrix}, \begin{bmatrix}\mathbf{b}_z \\ \mathbf{b}_w\end{bmatrix}\right\}, \tag{11}$$

$$Z \cap_{\mathbf{R}} Y = \left\{\begin{bmatrix}\mathbf{G}_z & \mathbf{0}\end{bmatrix}, \mathbf{c}_z, \begin{bmatrix}\mathbf{A}_z & \mathbf{0} \\ \mathbf{0} & \mathbf{A}_y \\ \mathbf{R}\mathbf{G}_z & -\mathbf{G}_y\end{bmatrix}, \begin{bmatrix}\mathbf{b}_z \\ \mathbf{b}_y \\ \mathbf{c}_y - \mathbf{R}\mathbf{c}_z\end{bmatrix}\right\}. \tag{12}$$

Unlike ellipsoids, parallelotopes, convex polytopes, and zonotopes, the operations (10)–(12) can be computed trivially and exactly with constrained zonotopes and result in only a mild increase in the complexity of the CG-rep (6). In addition, efficient complexity reduction methods are available in Scott et al. (2016) that enclose a constrained zonotope within another one with fewer generators and constraints, allowing one to balance accuracy and computational efficiency.

The methods developed in this paper also require some concepts from interval arithmetic, which are briefly recalled next. Let the set of compact intervals in $\mathbb{R}$ be denoted by $\mathbb{IR}$. An interval $X = [x^{\mathrm{L}}, x^{\mathrm{U}}] \in \mathbb{IR}$ is defined by $X \triangleq \{a \in \mathbb{R} : x^{\mathrm{L}} \leq a \leq x^{\mathrm{U}}\}$. The midpoint and radius are defined by $\mathrm{mid}(X) \triangleq \frac{1}{2}(x^{\mathrm{U}} + x^{\mathrm{L}})$ and $\mathrm{rad}(X) \triangleq \frac{1}{2}(x^{\mathrm{U}} - x^{\mathrm{L}})$. Interval vectors and matrices are defined by $\{\mathbf{a} \in \mathbb{R}^n : a_i^{\mathrm{L}} \leq a_i \leq a_i^{\mathrm{U}}\}$ and $\{\mathbf{A} \in \mathbb{R}^{n \times m} : A_{ij}^{\mathrm{L}} \leq A_{ij} \leq A_{ij}^{\mathrm{U}}\}$, respectively, with the midpoint and radius defined component-wise. An interval vector $X \in \mathbb{IR}^n$ can be written in generator representation as $\mathrm{mid}(X) \oplus \mathrm{diag}(\mathrm{rad}(X))B_\infty^n = \{\mathrm{diag}(\mathrm{rad}(X)), \mathrm{mid}(X)\}$. For any bounded $X \subset \mathbb{R}^n$, let $\square X$ refer to the interval hull of X. See Moore et al. (2009) for a review on basic operations and classic methods using interval analysis. In this work, the interval hull $\square Z$ of a constrained zonotope Z is computed using linear programming (Rego et al., 2020; Scott et al., 2016).

Finally, the following theorem defines a useful operation $\triangleleft(\mathbf{J}, X)$ for computing a constrained zonotopic enclosure of the product of an interval matrix $\mathbf{J}$ with a constrained zonotope X.

Theorem 1 (*Rego et al., 2020*)**.** *Let $X = \{\mathbf{G}, \mathbf{c}, \mathbf{A}, \mathbf{b}\} \subset \mathbb{R}^m$ be a constrained zonotope with n_g generators and n_c constraints, let $\mathbf{J} \in \mathbb{IR}^{n \times m}$ be an interval matrix, and consider the set $S = \mathbf{J}X \triangleq \{\hat{\mathbf{J}}\mathbf{x} : \hat{\mathbf{J}} \in \mathbf{J}, \mathbf{x} \in X\} \subset \mathbb{R}^n$. Let $\bar{\mathbf{G}} \in \mathbb{R}^{n \times \bar{n}_g}$ and $\bar{\mathbf{c}} \in \mathbb{R}^n$ satisfy $X \subseteq \{\bar{\mathbf{G}}, \bar{\mathbf{c}}\}$, and let $\mathbf{m}$ be an interval vector such that $\mathbf{m} \supseteq (\mathbf{J} - \mathrm{mid}(\mathbf{J}))\bar{\mathbf{c}}$ and $\mathrm{mid}(\mathbf{m}) = \mathbf{0}$. Finally, let $\mathbf{P} \in \mathbb{R}^{n \times n}$ be a diagonal matrix defined by $P_{ii} = \mathrm{rad}(m_i) + \sum_{j=1}^{\bar{n}_g}\sum_{k=1}^{m} \mathrm{rad}(J_{ik})|\bar{G}_{kj}|$ for all $i = 1, 2, \ldots, n$. Then, S is contained in the* CZ-inclusion

$$S \subseteq \triangleleft(\mathbf{J}, X) \triangleq \mathrm{mid}(\mathbf{J})X \oplus \mathbf{P}B_\infty^n.$$

Remark 2. In the implementation of $\triangleleft(\mathbf{J}, X)$ used in this paper, $\{\bar{\mathbf{G}}, \bar{\mathbf{c}}\} \supseteq X$ is obtained by eliminating all constraints from X using the constraint elimination algorithm in Scott et al. (2016), and $\mathbf{m}$ is obtained by evaluating $(\mathbf{J} - \mathrm{mid}(\mathbf{J}))\bar{\mathbf{c}}$ in interval arithmetic.

4. Nonlinear state estimation

This section presents new methods for computing enclosures for each step in the extended prediction-update-consistency algorithm (3)–(5) using constrained zonotopes. The proposed recursive scheme is summarized in Algorithm 1. In this algorithm, complexity reduction methods can be used after each step to limit the set complexity increase. We begin with two core lemmas required for all three steps.

Lemma 1. *Let $\boldsymbol{\alpha} : \mathbb{R}^n \times \mathbb{R}^{n_w} \to \mathbb{R}^{n_\alpha}$ be of class $\mathcal{C}^1$ and let $\nabla_x\boldsymbol{\alpha}$ denote the gradient of $\boldsymbol{\alpha}$ with respect to its first argument. Let $X \subset \mathbb{R}^n$ and*

[1] We drop the use of the superscript n_g for $B_\infty(\mathbf{A}_z, \mathbf{b}_z)$ since this dimension can be inferred from the number of columns of $\mathbf{A}_z$.

Algorithm 1 Proposed recursive algorithm

1: (Prediction step) Given the constrained zonotopes $\tilde{X}_{k-1} \times W \subset \mathbb{R}^n \times \mathbb{R}^{n_w}$, and input $\mathbf{u}_{k-1} \in \mathbb{R}^{n_u}$, compute the predicted constrained zonotope $\bar{X}_k$ satisfying (3).
2: (Update step) Given the constrained zonotopes $\bar{X}_k \times V \subset \mathbb{R}^n \times \mathbb{R}^{n_v}$, input $\mathbf{u}_k \in \mathbb{R}^{n_u}$, and measurement $\mathbf{y}_k \in \mathbb{R}^{n_y}$, compute a refined constrained zonotope $\hat{X}_k$ satisfying (4).
3: (Consistency step) Given the constrained zonotope $\hat{X}_k \subset \mathbb{R}^n$, compute a refined constrained zonotope $\tilde{X}_k$ satisfying (5).

$W \subset \mathbb{R}^{n_w}$ be constrained zonotopes, and let $\mathbf{J} \in \mathbb{IR}^{n \times n}$ be an interval matrix satisfying

$$\nabla_x^T \boldsymbol{\alpha}(\square X, W) \triangleq \{\nabla_x^T \boldsymbol{\alpha}(\mathbf{x}, \mathbf{w}) : \mathbf{x} \in \square X, \ \mathbf{w} \in W\} \subseteq \mathbf{J}. \tag{13}$$

For every $\mathbf{x} \in X$, $\mathbf{w} \in W$, and $\boldsymbol{\gamma}_x \in \square X$, there exists $\hat{\mathbf{J}} \in \mathbf{J}$ such that

$$\boldsymbol{\alpha}(\mathbf{x}, \mathbf{w}) = \boldsymbol{\alpha}(\boldsymbol{\gamma}_x, \mathbf{w}) + \hat{\mathbf{J}}(\mathbf{x} - \boldsymbol{\gamma}_x).$$

Proof. Choose any $(\mathbf{x}, \mathbf{w}) \in X \times W$. Since $\mathbf{x} \in X \subseteq \square X$ and $\gamma_x \in \square X$, the Mean Value Theorem ensures that, for any $i = 1, 2, \ldots, n$, $\exists \boldsymbol{\delta}^{[i]} \in \square X$ such that $\alpha_i(\mathbf{x}, \mathbf{w}) = \alpha_i(\boldsymbol{\gamma}_x, \mathbf{w}) + \nabla_x^T \alpha_i(\boldsymbol{\delta}^{[i]}, \mathbf{w})(\mathbf{x} - \boldsymbol{\gamma}_x)$. But $\nabla_x^T \alpha_i(\boldsymbol{\delta}^{[i]}, \mathbf{w})$ is contained in the ith row of $\mathbf{J}$ by hypothesis, and since this is true for all $i = 1, 2, \ldots, n$, $\exists \hat{\mathbf{J}} \in \mathbf{J}$ such that $\boldsymbol{\alpha}(\mathbf{x}, \mathbf{w}) = \boldsymbol{\alpha}(\boldsymbol{\gamma}_x, \mathbf{w}) + \hat{\mathbf{J}}(\mathbf{x} - \boldsymbol{\gamma}_x)$. ■

Remark 3. As with $\nabla_x^T \boldsymbol{\alpha}(\square X, W)$ in (13), real-valued functions written with set-valued arguments will henceforth always denote the true image set, rather than, e.g. an interval extension or other enclosure.

Lemma 1 provides an exact linear representation of the nonlinear function $\boldsymbol{\alpha}$ between two points based on the Mean Value Theorem, which is useful for computations with constrained zonotopes. This lemma is very similar to Theorem 2 in Rego et al. (2020). The only difference is that Theorem 2 in Rego et al. (2020) requires the approximation point $\boldsymbol{\gamma}_x$ to lie in X, while Lemma 1 allows $\boldsymbol{\gamma}_x$ to be chosen from the larger set $\square X$. This is important because obtaining a point in X (or testing a given point for membership) requires solving a linear program, whereas obtaining point in $\square X$ is trivial. The proof of Lemma 1 is given above for completeness, but it follows easily from the proof of Theorem 2 in Rego et al. (2020) by replacing the condition $\boldsymbol{\gamma}_x \in X$ with $\boldsymbol{\gamma}_x \in \square X$ throughout.[2]

The next lemma provides an alternative method for obtaining an exact linear representation of a nonlinear function between two points based on Taylor's Theorem. This lemma is similar to Theorem 3 in Rego et al. (2020), with the difference again that the approximation point is chosen from $\square Z$ rather than Z. The following notation is required. For a function $\boldsymbol{\beta} : \mathbb{R}^m \to \mathbb{R}^n$ of class $\mathcal{C}^2$ with qth component β_q and argument $\mathbf{z}$, let $\mathbf{H}\beta_q$ denote the upper triangular matrix describing half of the Hessian of β_q. Specifically, $H_{ii}\beta_q = (1/2)\partial^2 \beta_q / \partial z_i^2$, $H_{ij}\beta_q = \partial^2 \beta_q / \partial z_i \partial z_j$ for $i < j$, and $H_{ij}\beta_q = 0$ for $i > j$.

Lemma 2. *Let $\boldsymbol{\beta} : \mathbb{R}^m \to \mathbb{R}^n$ be of class $\mathcal{C}^2$ and let $\mathbf{z} \in \mathbb{R}^m$ denote its argument. Let $Z = \{\mathbf{G}, \mathbf{c}, \mathbf{A}, \mathbf{b}\} \subset \mathbb{R}^m$ be a constrained zonotope with m_g generators and m_c constraints. For each $q = 1, 2, \ldots, n$, let $\mathbf{Q}^{[q]} \in \mathbb{IR}^{m \times m}$ and $\tilde{\mathbf{Q}}^{[q]} \in \mathbb{IR}^{m_g \times m_g}$ be interval matrices satisfying $\mathbf{Q}^{[q]} \supseteq \mathbf{H}\beta_q(\square Z)$ and $\tilde{\mathbf{Q}}^{[q]} \supseteq \mathbf{G}^T \mathbf{Q}^{[q]} \mathbf{G}$. Moreover, define*

$$\tilde{c}_q = trace\left\{mid(\tilde{\mathbf{Q}}^{[q]})\right\}/2,$$

$$\tilde{\mathbf{G}}_{q,:} = \Big[\ \cdots \underbrace{mid(\tilde{Q}_{ii}^{[q]})/2}_{\forall i} \cdots \underbrace{\left(mid(\tilde{Q}_{ij}^{[q]}) + mid(\tilde{Q}_{ji}^{[q]})\right)}_{\forall i<j} \cdots \Big],$$

$$\tilde{\mathbf{G}}_{\mathbf{d}} = diag(\mathbf{d}), \quad d_q = \sum_{i,j} \left| rad(\tilde{Q}_{ij}^{[q]}) \right|, \quad \tilde{\mathbf{A}} = \left[\tilde{\mathbf{A}}_{\zeta} \ \tilde{\mathbf{A}}_{\xi} \ \mathbf{0}_{\frac{m_c}{2}(1+m_c) \times n}\right],$$

$$\tilde{\mathbf{A}}_{\zeta} = \begin{bmatrix} \vdots \\ \cdots \frac{1}{2} A_{ri} A_{si} \cdots \\ \vdots \end{bmatrix}_{\forall r \le s}, \quad \tilde{\mathbf{b}} = \begin{bmatrix} \vdots \\ b_r b_s - \frac{1}{2} \sum_i A_{ri} A_{si} \\ \vdots \end{bmatrix}_{\forall r \le s},$$

$$\tilde{\mathbf{A}}_{\xi} = \begin{bmatrix} \vdots \\ \cdots A_{ri} A_{sj} + A_{rj} A_{si} \cdots \\ \vdots \end{bmatrix}_{\forall r \le s},$$

with indices $i, j = 1, 2, \ldots, m_g$ and $r, s = 1, 2, \ldots, m_c$. Finally, choose any $\boldsymbol{\gamma}_z \in \square Z$ and let $\mathbf{L} \in \mathbb{IR}^{n \times m}$ be an interval matrix satisfying $\mathbf{L}_{q,:} \supseteq (\mathbf{c} - \boldsymbol{\gamma}_z)^T \mathbf{Q}^{[q]}$ for all $q = 1, \ldots, n$. For every $\mathbf{z} \in Z$, there exist $\boldsymbol{\xi} \in B_\infty(\mathbf{A}, \mathbf{b})$, $\tilde{\boldsymbol{\xi}} \in B_\infty(\tilde{\mathbf{A}}, \tilde{\mathbf{b}})$, and $\hat{\mathbf{L}} \in \mathbf{L}$ such that

$$\begin{aligned} \boldsymbol{\beta}(\mathbf{z}) = \boldsymbol{\beta}(\boldsymbol{\gamma}_z) + \nabla^T \boldsymbol{\beta}(\boldsymbol{\gamma}_z)(\mathbf{z} - \boldsymbol{\gamma}_z) \\ + \tilde{\mathbf{c}} + [\tilde{\mathbf{G}} \ \tilde{\mathbf{G}}_{\mathbf{d}}]\tilde{\boldsymbol{\xi}} + \hat{\mathbf{L}}((\mathbf{c} - \boldsymbol{\gamma}_z) + 2\mathbf{G}\boldsymbol{\xi}). \end{aligned}$$

Proof. This follows by replacing $\boldsymbol{\gamma}_z \in Z$ with $\boldsymbol{\gamma}_z \in \square Z$ in the proof of Theorem 3 in Rego et al. (2020). ■

4.1. Prediction step

This section presents two different approaches for the prediction step in Algorithm 1. The methods below are improved versions of the mean value and first-order Taylor extensions developed in Rego et al. (2020), respectively, which allow for a more flexible choice of the approximation point enabled by Lemmas 1 and 2. The proofs can be found in Appendix A.

Proposition 1. *Let $\mathbf{f} : \mathbb{R}^n \times \mathbb{R}^{n_u} \times \mathbb{R}^{n_w} \to \mathbb{R}^n$ be of class $\mathcal{C}^1$ and let $\nabla_x \mathbf{f}$ denote the gradient of $\mathbf{f}$ with respect to its first argument. Let $\mathbf{u} \in \mathbb{R}^{n_u}$, and let $X \subset \mathbb{R}^n$ and $W \subset \mathbb{R}^{n_w}$ be constrained zonotopes. Choose any $\boldsymbol{\gamma}_x \in \square X$. If Z_w is a constrained zonotope such that $\mathbf{f}(\boldsymbol{\gamma}_x, \mathbf{u}, W) \subseteq Z_w$ and $\mathbf{J} \in \mathbb{IR}^{n \times n}$ is an interval matrix satisfying $\nabla_x^T \mathbf{f}(\square X, \mathbf{u}, W) \subseteq \mathbf{J}$, then $\mathbf{f}(X, \mathbf{u}, W) \subseteq Z_w \oplus \triangleleft(\mathbf{J}, X - \boldsymbol{\gamma}_x)$.*

Proposition 2. *Let $\mathbf{f} : \mathbb{R}^n \times \mathbb{R}^{n_u} \times \mathbb{R}^{n_w} \to \mathbb{R}^n$ be of class $\mathcal{C}^2$, let $\mathbf{u} \in \mathbb{R}^{n_u}$, and let $X = \{\mathbf{G}_x, \mathbf{c}_x, \mathbf{A}_x, \mathbf{b}_x\}$ and $W = \{\mathbf{G}_w, \mathbf{c}_w, \mathbf{A}_w, \mathbf{b}_w\}$ be constrained zonotopes with (n_g, n_{g_w}) generators, and (n_c, n_{c_w}) constraints, respectively. Denote $\mathbf{z} = (\mathbf{x}, \mathbf{w})$ and $Z = X \times W = \{\mathbf{G}, \mathbf{c}, \mathbf{A}, \mathbf{b}\} \subset \mathbb{R}^{n+n_w}$. For each $q = 1, 2, \ldots, n$, let $\mathbf{Q}^{[q]} \in \mathbb{IR}^{(n+n_w)\times(n+n_w)}$ and $\tilde{\mathbf{Q}}^{[q]} \in \mathbb{IR}^{(n_g+n_{g_w})\times(n_g+n_{g_w})}$ be interval matrices satisfying $\mathbf{Q}^{[q]} \supseteq \mathbf{H}_z f_q(\square X, \mathbf{u}, \square W)$ and $\tilde{\mathbf{Q}}^{[q]} \supseteq \mathbf{G}^T \mathbf{Q}^{[q]} \mathbf{G}$. Moreover, define $\tilde{\mathbf{c}}$, $\tilde{\mathbf{G}}$, $\tilde{\mathbf{G}}_{\mathbf{d}}$, $\tilde{\mathbf{A}}$, and $\tilde{\mathbf{b}}$, as in Lemma 2. Finally, choose any $\boldsymbol{\gamma}_z = (\boldsymbol{\gamma}_x, \boldsymbol{\gamma}_w) \in \square Z$ and let $\mathbf{L} \in \mathbb{IR}^{n \times m}$ be an interval matrix satisfying $\mathbf{L}_{q,:} \supseteq (\mathbf{c} - \boldsymbol{\gamma}_z)^T \mathbf{Q}^{[q]}$ for all $q = 1, \ldots, n$. Then,*

$$\mathbf{f}(X, \mathbf{u}, W) \subseteq \mathbf{f}(\boldsymbol{\gamma}_x, \mathbf{u}, \boldsymbol{\gamma}_w) \oplus \nabla_z^T \mathbf{f}(\boldsymbol{\gamma}_x, \mathbf{u}, \boldsymbol{\gamma}_w)(Z - \boldsymbol{\gamma}_z) \oplus R, \tag{14}$$

where $R = \tilde{\mathbf{c}} \oplus \left[\tilde{\mathbf{G}} \ \tilde{\mathbf{G}}_{\mathbf{d}}\right] B_\infty(\tilde{\mathbf{A}}, \tilde{\mathbf{b}}) \oplus \triangleleft(\mathbf{L}, (\mathbf{c} - \boldsymbol{\gamma}_z) \oplus 2\mathbf{G}B_\infty(\mathbf{A}, \mathbf{b}))$.

Remark 4. The constrained zonotope Z_w in Proposition 1 can be obtained using the mean value extension $\mathbf{f}(\boldsymbol{\gamma}_x, \mathbf{u}, W) \subseteq Z_w = \mathbf{f}(\boldsymbol{\gamma}_x, \mathbf{u}, \boldsymbol{\gamma}_w) \oplus \triangleleft(\mathbf{J}_w, W - \boldsymbol{\gamma}_w)$ for a chosen point $\boldsymbol{\gamma}_w \in \square W$, with $\mathbf{J}_w$ being an interval matrix satisfying $\mathbf{J}_w \supseteq \nabla_w^T \mathbf{f}(\boldsymbol{\gamma}_x, \mathbf{u}, \square W)$. In this paper, the interval matrices $\mathbf{J}$, $\mathbf{J}_w$ (Proposition 1), $\mathbf{Q}^{[q]}$, $\tilde{\mathbf{Q}}^{[q]}$, $\mathbf{L}$

[2] In Rego et al. (2020) $\boldsymbol{\gamma}_x$ was denoted by $\mathbf{h}$.

(Proposition 2), and similar interval matrices in Propositions 3–4 and Corollaries 1–2, are all computed using interval arithmetic.

Remark 5. The complexity of the enclosures obtained by Propositions 1 and 2 are similar to the methods in Rego et al. (2020). Specifically, if X and W have n_g and n_{g_w} generators, and n_c and n_{c_w} constraints, respectively, then Proposition 1 gives $n_g + n_{g_w} + 2n$ generators and $n_c + n_{c_w}$ constraints, and Proposition 2 gives $0.5(n_g + n_{g_w})^2 + 2.5(n_g + n_{g_w}) + 2n$ generators and $0.5(n_c + n_{c_w})^2 + 2.5(n_c + n_{c_w})$ constraints.

Propositions 1 and 2 permit $\boldsymbol{\gamma}_x$ and $\boldsymbol{\gamma}_z$ to be chosen from $\square X$ and $\square Z$, respectively, whereas the corresponding results in Rego et al. (2020) required these points to be chosen from the smaller sets X and Z. The following example illustrates the potential advantage of these extensions.

Consider the nonlinear mapping $\mathbf{f} : \mathbb{R}^2 \to \mathbb{R}^2$ defined by

$$f_1(\mathbf{x}) = 3x_1 - \frac{x_1^2}{7} - \frac{4x_1x_2}{4+x_1}, \quad f_2(\mathbf{x}) = -2x_2 + \frac{3x_1x_2}{4+x_1}, \tag{15}$$

and the constrained zonotope

$$X = \left\{ \begin{bmatrix} 0.5 & 1 & -0.5 \\ 0.5 & 0.5 & 0 \end{bmatrix}, \begin{bmatrix} 5 \\ 0.5 \end{bmatrix}, \begin{bmatrix} -1 & 1 & -1 \end{bmatrix}, 2 \right\}.$$

As shown in Fig. 1, the center $\mathbf{c}$ in this CG-rep of X does not actually lie in X, but does lie in $\square X$. Therefore, it is a valid choice of $\boldsymbol{\gamma}_x$ in Proposition 2 here, but not in Theorem 3 in Rego et al. (2020). Fig. 1 shows the enclosures of $\mathbf{f}(X)$ obtained using Proposition 2 with this choice of $\boldsymbol{\gamma}_x$ and using Theorem 3 in Rego et al. (2020) with $\boldsymbol{\gamma}_x$ chosen as the closest point in X to $\mathbf{c}$, which is the best heuristic proposed in Rego et al. (2020). The enclosure obtained using Proposition 2 is tighter. Thus, allowing $\boldsymbol{\gamma}_x$ to lie in $\square X$ can lead to less conservative results.

4.2. Update step

This section presents both mean value and first-order Taylor methods for the update step in Algorithm 1, considering nonlinear measurement equations in contrast to the linear update step used in Rego et al. (2020). Specifically, Lemmas 1 and 2 are used, respectively, to formulate the required enclosure in (4) as the generalized intersection of two constrained zonotopes.

Proposition 3. *Let $\mathbf{g} : \mathbb{R}^n \times \mathbb{R}^{n_u} \times \mathbb{R}^{n_v} \to \mathbb{R}^{n_y}$ be of class $\mathcal{C}^1$, let $\mathbf{u} \in \mathbb{R}^{n_u}$, let $X \subset \mathbb{R}^n$ and $V \subset \mathbb{R}^{n_v}$ be constrained zonotopes, and choose any $\mathbf{y} \in \mathbb{R}^{n_y}$ such that $\mathbf{y} = \mathbf{g}(\mathbf{x}, \mathbf{u}, \mathbf{v})$ for some $(\mathbf{x}, \mathbf{v}) \in X \times V$. Choose any $\boldsymbol{\gamma}_x \in \square X$ and any $\tilde{\mathbf{J}} \in \mathbb{R}^{n_y \times n}$. If Z_v is a constrained zonotope such that $-\mathbf{g}(\boldsymbol{\gamma}_x, \mathbf{u}, V) \subseteq Z_v$, and $\mathbf{J} \in \mathbb{IR}^{n_y \times n}$ is an interval matrix satisfying $\nabla_x^T \mathbf{g}(\square X, \mathbf{u}, V) \subseteq \mathbf{J}$, then*

$$\{\mathbf{x} \in X : \mathbf{g}(\mathbf{x}, \mathbf{u}, \mathbf{v}) = \mathbf{y},\ \mathbf{v} \in V\} \subseteq X \cap_{\mathbf{C}} Y,$$

where $\mathbf{C} = \tilde{\mathbf{J}}$, and $Y = (\mathbf{y} + \tilde{\mathbf{J}}\boldsymbol{\gamma}_x) \oplus Z_v \oplus \triangleleft(\tilde{\mathbf{J}} - \mathbf{J}, X - \boldsymbol{\gamma}_x)$.

Proof. Choose any $(\mathbf{x}, \mathbf{v}) \in X \times V$ satisfying $\mathbf{g}(\mathbf{x}, \mathbf{u}, \mathbf{v}) = \mathbf{y}$. Lemma 1 ensures that there exists a real matrix $\hat{\mathbf{J}} \in \mathbf{J}$ such that $\mathbf{g}(\mathbf{x}, \mathbf{u}, \mathbf{v}) = \mathbf{g}(\boldsymbol{\gamma}_x, \mathbf{u}, \mathbf{v}) + \hat{\mathbf{J}}(\mathbf{x} - \boldsymbol{\gamma}_x)$. Since $\hat{\mathbf{J}} = \tilde{\mathbf{J}} + (\hat{\mathbf{J}} - \tilde{\mathbf{J}})$ holds, then $\mathbf{g}(\mathbf{x}, \mathbf{u}, \mathbf{v}) = \mathbf{g}(\boldsymbol{\gamma}_x, \mathbf{u}, \mathbf{v}) + \tilde{\mathbf{J}}(\mathbf{x} - \boldsymbol{\gamma}_x) + (\hat{\mathbf{J}} - \tilde{\mathbf{J}})(\mathbf{x} - \boldsymbol{\gamma}_x)$. Consequently,

$$\begin{aligned} \tilde{\mathbf{J}}\mathbf{x} &= \mathbf{g}(\mathbf{x}, \mathbf{u}, \mathbf{v}) + \tilde{\mathbf{J}}\boldsymbol{\gamma}_x - \mathbf{g}(\boldsymbol{\gamma}_x, \mathbf{u}, \mathbf{v}) + (\tilde{\mathbf{J}} - \hat{\mathbf{J}})(\mathbf{x} - \boldsymbol{\gamma}_x) \\ &= \mathbf{y} + \tilde{\mathbf{J}}\boldsymbol{\gamma}_x - \mathbf{g}(\boldsymbol{\gamma}_x, \mathbf{u}, \mathbf{v}) + (\tilde{\mathbf{J}} - \hat{\mathbf{J}})(\mathbf{x} - \boldsymbol{\gamma}_x) \\ &\in (\mathbf{y} + \tilde{\mathbf{J}}\boldsymbol{\gamma}_x) \oplus Z_v \oplus \triangleleft(\tilde{\mathbf{J}} - \mathbf{J}, X - \boldsymbol{\gamma}_x) = Y. \end{aligned}$$

Then, we conclude that $\{\mathbf{x} \in X : \mathbf{g}(\mathbf{x}, \mathbf{u}, \mathbf{v}) = \mathbf{y}, \mathbf{v} \in V\} \subseteq \{\mathbf{x} \in X : \tilde{\mathbf{J}}\mathbf{x} \in Y\} = X \cap_{\mathbf{C}} Y$. ■

Remark 6. The constrained zonotope Z_v in Proposition 3 can be obtained as $Z_v = -\mathbf{g}(\boldsymbol{\gamma}_x, \mathbf{u}, \boldsymbol{\gamma}_v) \oplus \triangleleft\left(-\mathbf{J}_v, V - \boldsymbol{\gamma}_v\right) \supseteq -\mathbf{g}(\boldsymbol{\gamma}_x, \mathbf{u}, V)$ for some $\boldsymbol{\gamma}_v \in \square V$ and interval matrix $\mathbf{J}_v \supseteq \nabla_v^T \mathbf{g}(\boldsymbol{\gamma}_x, \mathbf{u}, \square V)$. The matrix $\tilde{\mathbf{J}}$ is a free parameter in Proposition 3. Choosing $\tilde{\mathbf{J}} = \text{mid}(\mathbf{J})$ gives $\text{mid}(\tilde{\mathbf{J}} - \mathbf{J}) = \mathbf{0}$, and hence $\triangleleft(\tilde{\mathbf{J}} - \mathbf{J}, X - \boldsymbol{\gamma}_x) = \text{mid}(\tilde{\mathbf{J}} - \mathbf{J})(X - \boldsymbol{\gamma}_x) \oplus \mathbf{P}B_\infty^{n_y} = \mathbf{P}B_\infty^{n_y}$, with $\mathbf{P}$ defined as in Theorem 1. This choice is adopted throughout this paper.

Proposition 4. *Let $\mathbf{g} : \mathbb{R}^n \times \mathbb{R}^{n_u} \times \mathbb{R}^{n_v} \to \mathbb{R}^{n_y}$ be of class $\mathcal{C}^2$, let $\mathbf{u} \in \mathbb{R}^{n_u}$, let $X = \{\mathbf{G}_x, \mathbf{c}_x, \mathbf{A}_x, \mathbf{b}_x\}$ and $V = \{\mathbf{G}_v, \mathbf{c}_v, \mathbf{A}_v, \mathbf{b}_v\}$ be constrained zonotopes with (n_g, n_{g_v}) generators, and (n_c, n_{c_v}) constraints, respectively, and choose any $\mathbf{y} \in \mathbb{R}^{n_y}$ such that $\mathbf{y} = \mathbf{g}(\mathbf{x}, \mathbf{u}, \mathbf{v})$ for some $(\mathbf{x}, \mathbf{v}) \in X \times V$. Denote $\mathbf{z} = (\mathbf{x}, \mathbf{v})$ and $Z = X \times V = \{\mathbf{G}, \mathbf{c}, \mathbf{A}, \mathbf{b}\} \subset \mathbb{R}^{n+n_v}$. For each $q = 1, 2, \ldots, n_y$, let $\mathbf{Q}^{[q]} \in \mathbb{IR}^{(n+n_v)\times(n+n_v)}$ and $\tilde{\mathbf{Q}}^{[q]} \in \mathbb{IR}^{(n_g+n_{g_v})\times(n_g+n_{g_v})}$ be interval matrices satisfying $\mathbf{Q}^{[q]} \supseteq \mathbf{H}_z g_q(\square X, \mathbf{u}, \square V)$ and $\tilde{\mathbf{Q}}^{[q]} \supseteq \mathbf{G}^T \mathbf{Q}^{[q]} \mathbf{G}$. Moreover, define $\tilde{\mathbf{c}}$, $\tilde{\mathbf{G}}$, $\tilde{\mathbf{G}}_\mathbf{d}$, $\tilde{\mathbf{A}}$, and $\tilde{\mathbf{b}}$, as in Lemma 2. Finally, choose any $\boldsymbol{\gamma}_z = (\boldsymbol{\gamma}_x, \boldsymbol{\gamma}_v) \in \square Z$ and let $\mathbf{L} \in \mathbb{IR}^{n_y \times (n+n_v)}$ be an interval matrix satisfying $\mathbf{L}_{q,:} \supseteq (\mathbf{c} - \boldsymbol{\gamma}_z)^T \mathbf{Q}^{[q]}$ for all $q = 1, \ldots, n_y$. Then,*

$$\{\mathbf{x} \in X : \mathbf{g}(\mathbf{x}, \mathbf{u}, \mathbf{v}) = \mathbf{y},\ \mathbf{v} \in V\} \subseteq X \cap_{\mathbf{C}} Y,$$

where $\mathbf{C} = \nabla_x^T \mathbf{g}(\boldsymbol{\gamma}_x, \mathbf{u}, \boldsymbol{\gamma}_v)$, $Y = (\mathbf{y} - \mathbf{g}(\boldsymbol{\gamma}_x, \mathbf{u}, \boldsymbol{\gamma}_v) + \nabla_z^T \mathbf{g}(\boldsymbol{\gamma}_x, \mathbf{u}, \boldsymbol{\gamma}_v)\boldsymbol{\gamma}_z) \oplus (-\nabla_v^T \mathbf{g}(\boldsymbol{\gamma}_x, \mathbf{u}, \boldsymbol{\gamma}_v)V) \oplus (-R)$, and $R = \tilde{\mathbf{c}} \oplus [\tilde{\mathbf{G}}\ \tilde{\mathbf{G}}_\mathbf{v}] B_\infty(\tilde{\mathbf{A}}, \tilde{\mathbf{b}}) \oplus \triangleleft(\mathbf{L}, (\mathbf{c} - \boldsymbol{\gamma}_z) \oplus 2\mathbf{G}B_\infty(\mathbf{A}, \mathbf{b}))$.

Proof. Choose $(\mathbf{x}, \mathbf{v}) = \mathbf{z} \in Z$ such that $\mathbf{g}(\mathbf{x}, \mathbf{u}, \mathbf{v}) = \mathbf{y}$. Lemma 2 ensures that there exist $\boldsymbol{\xi} \in B_\infty(\mathbf{A}, \mathbf{b})$, $\tilde{\boldsymbol{\xi}} \in B_\infty(\tilde{\mathbf{A}}, \tilde{\mathbf{b}})$, and $\hat{\mathbf{L}} \in \mathbf{L}$, such that

$$\begin{aligned} \mathbf{g}(\mathbf{x}, \mathbf{u}, \mathbf{v}) = \mathbf{g}(\boldsymbol{\gamma}_x, \mathbf{u}, \boldsymbol{\gamma}_v) &+ \nabla_x^T \mathbf{g}(\boldsymbol{\gamma}_x, \mathbf{u}, \boldsymbol{\gamma}_v)(\mathbf{x} - \boldsymbol{\gamma}_x) \\ &+ \nabla_v^T \mathbf{g}(\boldsymbol{\gamma}_x, \mathbf{u}, \boldsymbol{\gamma}_v)(\mathbf{v} - \boldsymbol{\gamma}_v) + \hat{\mathbf{L}}(\mathbf{p} + 2\mathbf{G}\boldsymbol{\xi}) + \tilde{\mathbf{c}} + [\tilde{\mathbf{G}}\ \tilde{\mathbf{G}}_\mathbf{v}]\tilde{\boldsymbol{\xi}}. \end{aligned}$$

where $\mathbf{p} = \mathbf{c} - \boldsymbol{\gamma}_z$. Since $\mathbf{g}(\mathbf{x}, \mathbf{u}, \mathbf{v}) = \mathbf{y}$,

$$\begin{aligned} \nabla_x^T \mathbf{g}(\boldsymbol{\gamma}_x, \mathbf{u}, \boldsymbol{\gamma}_v)\mathbf{x} &= \mathbf{y} - \mathbf{g}(\boldsymbol{\gamma}_x, \mathbf{u}, \boldsymbol{\gamma}_v) + \nabla_z^T \mathbf{g}(\boldsymbol{\gamma}_x, \mathbf{u}, \boldsymbol{\gamma}_v)\boldsymbol{\gamma}_z \\ &\quad - \nabla_v^T \mathbf{g}(\boldsymbol{\gamma}_x, \mathbf{u}, \boldsymbol{\gamma}_v)\mathbf{v} - \hat{\mathbf{L}}(\mathbf{p} + 2\mathbf{G}\boldsymbol{\xi}) - \tilde{\mathbf{c}} - [\tilde{\mathbf{G}}\ \tilde{\mathbf{G}}_\mathbf{v}]\tilde{\boldsymbol{\xi}} \\ &\in (\mathbf{y} - \mathbf{g}(\boldsymbol{\gamma}_x, \mathbf{u}, \boldsymbol{\gamma}_v) + \nabla_z^T \mathbf{g}(\boldsymbol{\gamma}_x, \mathbf{u}, \boldsymbol{\gamma}_v)\boldsymbol{\gamma}_z) \\ &\quad \oplus (-\nabla_v^T \mathbf{g}(\boldsymbol{\gamma}_x, \mathbf{u}, \boldsymbol{\gamma}_v)V) \oplus (-R) = Y \end{aligned}$$

Then, we conclude that $\{\mathbf{x} \in X : \mathbf{g}(\mathbf{x}, \mathbf{u}, \mathbf{v}) = \mathbf{y}, \mathbf{v} \in V\} \subseteq \{\mathbf{x} \in X : \nabla_x^T \mathbf{g}(\boldsymbol{\gamma}_x, \mathbf{u}, \boldsymbol{\gamma}_v)\mathbf{x} \in Y\} = X \cap_{\mathbf{C}} Y$. ■

Remark 7. If X and V have n_g and n_{g_v} generators, and n_c and n_{c_v} constraints, respectively, then the enclosure obtained by Proposition 3 has $2n_g + n_{g_v} + 2n_y$ generators and $2n_c + n_{c_v} + n_y$ constraints, and the enclosure obtained by Proposition 4 has $0.5(n_g + n_{g_v})^2 + 2.5(n_g + n_{g_v}) + 2n_y$ generators and $0.5(n_c + n_{c_v})^2 + 2.5(n_c + n_{c_v}) + n_y$ constraints.

Remark 8. If $\mathbf{f}$ and $\mathbf{g}$ are affine in $\mathbf{w}$ and $\mathbf{v}$ (i.e., $\mathbf{f}(\mathbf{x}, \mathbf{u}, \mathbf{w}) = \boldsymbol{\phi}(\mathbf{x}, \mathbf{u}) + \Phi(\mathbf{x}, \mathbf{u})\mathbf{w}$ and $\mathbf{g}(\mathbf{x}, \mathbf{u}, \mathbf{v}) = \boldsymbol{\psi}(\mathbf{x}, \mathbf{u}) + \Psi(\mathbf{x}, \mathbf{u})\mathbf{v}$), then the constrained zonotopes $Z_w \supseteq \mathbf{f}(\boldsymbol{\gamma}_x, \mathbf{u}, W)$ and $Z_v \supseteq -\mathbf{g}(\boldsymbol{\gamma}_x, \mathbf{u}, V)$ in Propositions 1 and 3 can be computed exactly by $Z_w = \boldsymbol{\phi}(\boldsymbol{\gamma}_x, \mathbf{u}) \oplus \Phi(\boldsymbol{\gamma}_x, \mathbf{u})W$ and $Z_v = -\boldsymbol{\psi}(\boldsymbol{\gamma}_x, \mathbf{u}) \oplus (-\Psi(\boldsymbol{\gamma}_x, \mathbf{u})V)$, respectively.

4.3. Consistency step

This section presents both mean value and first-order Taylor methods for the consistency step in Algorithm 1. As in the previous section, the obtained enclosure is formulated as the generalized intersection of two constrained zonotopes. Since the proposed methods are direct consequences of Propositions 3 and 4, they are presented as corollaries.

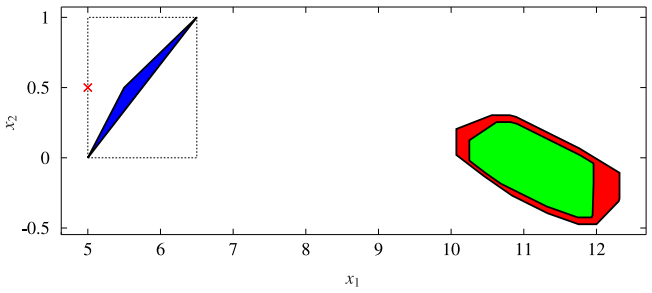

Fig. 1. The sets X (blue), $\square X$ (dashed lines), the center of X ($\times$), the enclosures obtained using Proposition 2 with $\boldsymbol{\gamma}_x$ as the center of X (green), and using Theorem 3 in Rego et al. (2020) with $\boldsymbol{\gamma}_x$ as the closest point in X to its center (red). (For interpretation of the references to color in this figure legend, the reader is referred to the web version of this article.)

Corollary 1. *Let $\mathbf{h} : \mathbb{R}^n \to \mathbb{R}^{n_h}$ be of class $\mathcal{C}^1$ and let $X \subset \mathbb{R}^n$ be a constrained zonotope. Choose any $\boldsymbol{\gamma}_x \in \square X$ and any $\tilde{\mathbf{J}} \in \mathbb{R}^{n_h \times n}$. If $\mathbf{J} \in \mathbb{IR}^{n_h \times n}$ is an interval matrix satisfying $\nabla_x^T \mathbf{h}(\square X) \subseteq \mathbf{J}$, then $\{\mathbf{x} \in X : \mathbf{h}(\mathbf{x}) = \mathbf{0}\} \subseteq X \cap_{\mathbf{D}} H$, where $\mathbf{D} = \tilde{\mathbf{J}}$, and $H = (\tilde{\mathbf{J}}\boldsymbol{\gamma}_x - \mathbf{h}(\boldsymbol{\gamma}_x)) \oplus \triangleleft(\tilde{\mathbf{J}} - \mathbf{J}, X - \boldsymbol{\gamma}_x)$.*

Proof. See Appendix A. ■

Remark 9. As in the update step, the matrix $\tilde{\mathbf{J}}$ is a free parameter in Corollary 1. If $\tilde{\mathbf{J}} = \text{mid}(\mathbf{J})$, then $\text{mid}(\tilde{\mathbf{J}} - \mathbf{J}) = \mathbf{0}$, and $\triangleleft(\tilde{\mathbf{J}} - \mathbf{J}, X - \boldsymbol{\gamma}_x) = \text{mid}(\tilde{\mathbf{J}} - \mathbf{J})(X - \boldsymbol{\gamma}_x) \oplus \mathbf{P}B_\infty^{n_y} = \mathbf{P}B_\infty^{n_y}$. Therefore, this choice is adopted also for the consistency step.

Corollary 2. *Let $\mathbf{h} : \mathbb{R}^n \to \mathbb{R}^{n_h}$ be of class $\mathcal{C}^2$ and let $X = \{\mathbf{G}, \mathbf{c}, \mathbf{A}, \mathbf{b}\}$ be a constrained zonotope with n_g generators and n_c constraints. For each $q = 1, 2, \ldots, n_h$, let $\mathbf{Q}^{[q]} \in \mathbb{IR}^{n \times n}$ and $\tilde{\mathbf{Q}}^{[q]} \in \mathbb{IR}^{n_g \times n_g}$ be interval matrices satisfying $\mathbf{Q}^{[q]} \supseteq \mathbf{H}_x h_q(\square X)$ and $\tilde{\mathbf{Q}}^{[q]} \supseteq \mathbf{G}^T \mathbf{Q}^{[q]} \mathbf{G}$. Moreover, define $\tilde{\mathbf{c}}$, $\tilde{\mathbf{G}}$, $\tilde{\mathbf{G}}_\mathbf{d}$, $\tilde{\mathbf{A}}$, and $\tilde{\mathbf{b}}$, as in Lemma 2. Finally, choose any $\boldsymbol{\gamma}_x \in \square X$ and let $\mathbf{L} \in \mathbb{IR}^{n_h \times n}$ be an interval matrix satisfying $\mathbf{L}_{q,:} \supseteq (\mathbf{c} - \boldsymbol{\gamma}_x)^T \mathbf{Q}^{[q]}$ for all $q = 1, \ldots, n_h$. Then,*

$$\{\mathbf{x} \in X : \mathbf{h}(\mathbf{x}) = \mathbf{0}\} \subseteq X \cap_{\mathbf{D}} H,$$

where $\mathbf{D} = \nabla_x^T \mathbf{h}(\boldsymbol{\gamma}_x)$, $H = (-\mathbf{h}(\boldsymbol{\gamma}_x) + \nabla_x^T \mathbf{h}(\boldsymbol{\gamma}_x)\boldsymbol{\gamma}_x) \oplus (-R)$, and $R = \tilde{\mathbf{c}} \oplus [\tilde{\mathbf{G}} \;\; \tilde{\mathbf{G}}_\mathbf{d}] B_\infty(\tilde{\mathbf{A}}, \tilde{\mathbf{b}}) \oplus \triangleleft(\mathbf{L}, (\mathbf{c} - \boldsymbol{\gamma}_x) \oplus 2\mathbf{G}B_\infty(\mathbf{A}, \mathbf{b}))$.

Proof. See Appendix A. ■

Remark 10. If X has n_g generators and n_c constraints, then the enclosure obtained from Corollary 1 has $2n_g + n_y$ generators and $2n_c + n_y$ constraints, and the enclosure obtained from Corollary 2 has $0.5n_g^2 + 2.5n_g + 2n_y$ generators and $0.5n_c^2 + 2.5n_c + n_y$ constraints.

Remark 11. The enclosures in Corollaries 1 and 2 can be tightened if an enclosure X_F in CG-rep of the feasible state set $\{\mathbf{x} \in \mathbb{R}^n : \mathbf{h}(\mathbf{x}) = \mathbf{0}\}$ is known *a priori*. Such an enclosure can be obtained offline by using, for instance, the contractor programming methods in Chabert and Jaulin (2009). In both corollaries, $\mathbf{h}$ is conservatively approximated over X, and the size of the resulting constrained zonotope Z is proportional to the size of X. If X is large, significant improvement can result from setting $X \leftarrow X \cap X_\text{F}$ prior to applying the corollary. This situation is likely in practice because, within the overall estimation framework (3)–(5), the set $\hat{X}_k$ will play the role of X in Corollaries 1 and 2, and $\hat{X}_k$ can be very conservative before accounting for the invariant $\mathbf{h}(\mathbf{x}_k) = \mathbf{0}$ (see Section 5.2).

Remark 12. Various alternative methods have previously been proposed for intersecting a given set with the solution set of a system of nonlinear equations; e.g., Kochdumper and Althoff (2020). However, none of these existing methods can be applied to sets described by constrained zonotopes, and the computed enclosures are generally nonconvex.

Remark 13. In practice, nonlinear invariants of the form $\mathbf{h}(\mathbf{x}_k) = \mathbf{0}$ may not hold exactly. However, inexact invariants can still be used by introducing an additional uncertain variable $\mathbf{d}_k \in \mathbb{R}^{n_d}$, bounded in a polytope $D \subset \mathbb{R}^{n_d}$, such that $\mathbf{h}(\mathbf{x}_k, \mathbf{d}_k) = \mathbf{0}$ holds. The resulting procedures are very similar to Propositions 3 and 4 with $\mathbf{y}_k \triangleq \mathbf{0}$, $\mathbf{v}_k \triangleq \mathbf{d}_k$, and $\mathbf{g} \triangleq \mathbf{h}$.

4.4. Selection of γ

The methods proposed in this paper require heuristics to choose a point $(\boldsymbol{\gamma}_x, \boldsymbol{\gamma}_w, \boldsymbol{\gamma}_v) \in \square X \times \square W \times \square V$, where X stands for either $\tilde{X}_{k-1}$, $\bar{X}_k$, or $\hat{X}_k$ depending on the step in (3)–(5). As discussed in Rego et al. (2020), the center of the CG-rep. of $X \times W \times V$ cannot be chosen in general because it may not belong to either $X \times W \times V$ or $\square X \times \square W \times \square V$. However, in contrast to Rego et al. (2020), the center of the interval $\square X \times \square W \times \square V$ is a valid choice here. This first heuristic is summarized as follows:

(C1) $(\boldsymbol{\gamma}_x, \boldsymbol{\gamma}_w, \boldsymbol{\gamma}_v)$ is given by the center of $\square X \times \square W \times \square V$.

Despite its efficiency, *C1* is not optimal in any sense and can lead to conservative enclosures. Following Rego et al. (2020), we next present an improved heuristic *C2* specifically for use with the methods based on mean value extensions in Propositions 1 and 3, and Corollary 1 (the exact heuristic in Rego et al. (2020) is not optimal here because it restricts $(\boldsymbol{\gamma}_x, \boldsymbol{\gamma}_w, \boldsymbol{\gamma}_v)$ to $X \times W \times V$ rather than $\square X \times \square W \times \square V$). Propositions 1 and 3, and Corollary 1 all apply the CZ-inclusion defined in Theorem 1 with the second argument taking the form $X - \boldsymbol{\gamma}_x$. The idea behind *C2* is therefore to choose $\boldsymbol{\gamma}_x$ so as to minimize the conservatism of this CZ-inclusion.

In this sense, consider the CZ-inclusion $\triangleleft(\mathbf{J}, Z - \boldsymbol{\gamma})$ for arbitrary $Z = \{\mathbf{G}, \mathbf{c}, \mathbf{A}, \mathbf{b}\} \subset \mathbb{R}^m$ and $\mathbf{J} \in \mathbb{IR}^{m \times n}$. As per Theorem 1 and Remark 2, computing $\triangleleft(\mathbf{J}, Z - \boldsymbol{\gamma})$ requires a zonotope $\{\bar{\mathbf{G}}, \bar{\mathbf{c}}\} \supseteq (Z - \boldsymbol{\gamma})$ that is computed by eliminating all constraints from $(Z - \boldsymbol{\gamma})$ using the constraint elimination algorithm in Scott et al. (2016). Based on that algorithm, Rego et al. (2020) derived a closed form expression for the resulting center $\bar{\mathbf{c}}$ as a function of $(\mathbf{G}, \mathbf{c}, \mathbf{A}, \mathbf{b})$ and $\boldsymbol{\gamma}$, which takes the form

$$\bar{\mathbf{c}} = \mathbf{c} - \boldsymbol{\gamma} + \delta(\mathbf{G}, \mathbf{A}, \mathbf{b}).$$

The definition of δ can be deduced from Lemma 1 in Rego et al. (2020) and is omitted here for brevity. This $\bar{\mathbf{c}}$ is then used to compute $\mathbf{m} \supset (\mathbf{J} - \text{mid}(\mathbf{J}))\bar{\mathbf{c}}$ using interval arithmetic, and the size of the final enclosure $\triangleleft(\mathbf{J}, Z - \boldsymbol{\gamma})$ is proportional to $\text{rad}(\mathbf{m}) = (1/2)\text{diam}(\mathbf{m})$. Thus, the aim is to choose $\boldsymbol{\gamma}$ so as to minimize $\text{diam}(\mathbf{m})$.

Proposition 5. *Let $Z = \{\mathbf{G}, \mathbf{c}, \mathbf{A}, \mathbf{b}\} \subset \mathbb{R}^m$, $\mathbf{J} \in \mathbb{IR}^{m \times n}$, and $[\mathbf{z}^L, \mathbf{z}^U] = \square Z$. For any choice of $\boldsymbol{\gamma} \in \square Z$, let $\mathbf{m}_\gamma \supseteq (\mathbf{J} - mid(\mathbf{J}))\bar{\mathbf{c}}_\gamma$ be an interval vector computed using interval arithmetic, where $\bar{\mathbf{c}}_\gamma = \mathbf{c} - \boldsymbol{\gamma} + \delta(\mathbf{G}, \mathbf{A}, \mathbf{b})$. Then $\boldsymbol{\gamma}^* \in \square Z$ minimizes $\|diam(\mathbf{m}_\gamma)\|_1$ iff it is the solution to the linear program (LP)*

$$\min_{\boldsymbol{\gamma}} \|\Theta \bar{\mathbf{c}}_\gamma\|_1, \quad s.t. \quad \mathbf{z}^L \le \boldsymbol{\gamma} \le \mathbf{z}^U, \tag{16}$$

where $\Theta_{ij} = \sum_{i=1}^m diam(J_{ij})$ and $\Theta_{ij} = 0$ for all $i \neq j$.

Proof. See Appendix A.

Table 1
Computational complexity $O(\cdot)$ of the prediction, update, and consistency steps using constrained zonotopes.

Step	Mean value extension	Simplified
Prediction	$nm_{w}m_{g_w} + (m_w m_{g_w} + m_{c_w})(m_{g_w} + m_{c_w})^3$	n^5
Update	$n_y(m_v m_{g_v} + n_y) + (m_v m_{g_v} + m_{c_v})(m_{g_v} + m_{c_v})^3$	n^5
Consistency	$n_h(n\hat{n}_g + n_h) + (n\hat{n}_g + \hat{n}_c)(\hat{n}_g + \hat{n}_c)^3$	n^5
Step	**First-order extension**	**Simplified**
Prediction	$n(m_w^2 m_{g_w} + m_w m_{g_w}^2) + (m_w m_{g_w} + m_{c_w})(m_{g_w} + m_{c_w})^3$	n^5
Update	$n_y^2 + n_y(m_v^2 m_{g_v} + m_v m_{g_v}^2) + (m_v m_{g_v} + m_{c_v})(m_{g_v} + m_{c_v})^3$	n^5
Consistency	$n_h^2 + n_h(n^2\hat{n}_g + n\hat{n}_g^2) + (n\hat{n}_g + \hat{n}_c)(\hat{n}_g + \hat{n}_c)^3$	n^5

This heuristic is summarized as follows:

(C2) $\boldsymbol{\gamma}_x$, $\boldsymbol{\gamma}_w$, and $\boldsymbol{\gamma}_v$ are given by the points obtained from Proposition 5 for $(\mathbf{J}, X-\boldsymbol{\gamma}_x)$ in Proposition 1, $(\tilde{\mathbf{J}}-\mathbf{J}, X-\boldsymbol{\gamma}_x)$ in Proposition 3 and Corollary 1, $(\mathbf{J}_w, W-\boldsymbol{\gamma}_w)$, and $(\mathbf{J}_v, V-\boldsymbol{\gamma}_v)$, respectively.

Next, we present a heuristic specifically for the methods based on first-order Taylor extensions in Propositions 2 and 4, and Corollary 2. The conservatism of these methods is directly related to the conservatism in the remainder R, which is mostly affected by the size of the interval matrices $\mathbf{Q}^{[q]}$, $\tilde{\mathbf{Q}}^{[q]}$, and $\mathbf{L}$. The matrices $\mathbf{Q}^{[q]}$ and $\tilde{\mathbf{Q}}^{[q]}$ are unaffected by the choice of $(\boldsymbol{\gamma}_x, \boldsymbol{\gamma}_w, \boldsymbol{\gamma}_v)$. However, the radius of $\mathbf{L}$ is proportional to the differences $\mathbf{c}_x - \boldsymbol{\gamma}_x$, $\mathbf{c}_w - \boldsymbol{\gamma}_w$, and $\mathbf{c}_v - \boldsymbol{\gamma}_v$. Therefore, we propose the following heuristic:

(C3) $(\boldsymbol{\gamma}_x, \boldsymbol{\gamma}_w, \boldsymbol{\gamma}_v)$ is the closest point to the center of $X \times W \times V$ that belongs to $\square X \times \square W \times \square V$, obtained by solving the respective LPs $\min\{\|\boldsymbol{\gamma} - \mathbf{c}_x\|_1 : \boldsymbol{\gamma} \in \square X\}$, $\min\{\|\boldsymbol{\gamma} - \mathbf{c}_w\|_1 : \boldsymbol{\gamma} \in \square W\}$, and $\min\{\|\boldsymbol{\gamma} - \mathbf{c}_v\|_1 : \boldsymbol{\gamma} \in \square V\}$.

Remark 14. In this section, we propose different heuristics to choose $(\boldsymbol{\gamma}_x, \boldsymbol{\gamma}_w, \boldsymbol{\gamma}_v)$ depending if the mean value extension or the first-order Taylor extension are used (*C2* and *C3*, respectively). This is because this choice affects the computed enclosure in different ways for the different extensions. See Rego et al. (2020) for a detailed motivation.

4.5. Computational complexity

Table 1 shows the computational complexity of our methods for the prediction, update, and consistency steps, using the mean value extension (Propositions 1 and 3, and Corollary 1) and the first-order Taylor extension (Propositions 2 and 4, and Corollary 2). To derive these complexities, we consider that the enclosures $(\tilde{X}_{k-1}, \bar{X}_k, \hat{X}_k)$ have $(\tilde{n}_g, \bar{n}_g, \hat{n}_g)$ generators and $(\tilde{n}_c, \bar{n}_c, \hat{n}_c)$ constraints, respectively. Moreover, (W, V) have (n_{g_w}, n_{g_v}) generators and (n_{c_w}, n_{c_v}) constraints, and we define $(m_w, m_{g_w}, m_{c_w}) \triangleq (n + n_w, \tilde{n}_g + n_{g_w}, \tilde{n}_c + n_{c_w})$, and $(m_v, m_{g_v}, m_{c_v}) \triangleq (n + n_v, \bar{n}_g + n_{g_v}, \bar{n}_c + n_{c_v})$. As in Rego et al. (2020), we assume that evaluations of nonlinear real functions and nonlinear inclusion functions have complexity $O(1)$, and that all LPs (including the ones necessary to compute the interval hulls) are solved at least with the performance of the method proposed in Kelner and Spielman (2006). This method has (simplified) polynomial complexity $O(N_d N_c^3)$, with N_d and N_c the number of decision variables and constraints, respectively.

The complexities of the prediction, update, and consistency steps, using the mean value and first-order Taylor extensions, are similar to the previous prediction methods proposed in Rego et al. (2020). In all the complexities shown in Table 1, the higher order terms such as $(m_w m_{g_w} + m_{c_w})(m_{g_w} + m_{c_w})^3$ come from both the interval hull computations and the constraint elimination procedure used to obtain the zonotope enclosure required by Theorem 1. The other terms come from matrix products that appear in the proposed expressions to compute the respective CG-rep variables.

Table 1 also shows a simplified complexity analysis of the proposed methods for each step. In this analysis, we consider that every variable is proportional to the space dimension n, and that $(\tilde{X}_{k-1}, \bar{X}_k, \hat{X}_k)$ have the same number of generators and constraints (this can be achieved by using generator reduction and constraint elimination methods after each step). Details on the complexities of the basic operations with constrained zonotopes are found in Rego et al. (2020).

5. Numerical examples

This section evaluates the accuracy of the set-valued state estimation methods proposed in Section 4. Let CZMV denote the method based entirely on the mean value extension, using Proposition 1 for the prediction step and Proposition 3 for the update step, but with no consistency step. Moreover, let CZMV+C denote the method CZMV with the addition the consistency step using Corollary 1, let CZMV+F denote CZMV with the addition of an intersection with an enclosure of the feasible state set as described in Remark 11, and let CZMV+FC denote CZMV with the addition of both the intersection in Remark 11 and then the consistency step using Corollary 1. These are referred to collectively as CZMV-like methods. Analogously, let CZFO denote the method based entirely on first-order Taylor extensions, using Proposition 2 for the prediction step and Proposition 4 for the update step, and let CZFO+C, CZFO+F, and CZFO+FC denote CZFO with the addition of, respectively, the consistency step using Corollary 2, the intersection described in Remark 11, and both the intersection and the consistency step. In CZMV-like methods, complexity reduction is applied after the consistency step using the reduction methods in Scott et al. (2016), with constraint elimination performed prior to generator reduction. Due to the quadratic complexity increase of the enclosure in each intermediate step of CZFO-like methods (see Remarks 5, 7 and 9), complexity reduction is applied after all three steps in these methods. Heuristic *C2* is used for choosing $(\boldsymbol{\gamma}_x, \boldsymbol{\gamma}_w, \boldsymbol{\gamma}_v)$ in CZMV-like methods, and heuristic *C3* in CZFO-like methods.

We also compare our results with two nonlinear zonotope methods with prediction steps based on the Mean Value Theorem in Alamo et al. (2005) and Taylor's Theorem in Combastel (2005). These are denoted by ZMV and ZFO,[3] respectively. In both zonotope methods, the nonlinear update step is given by the intersection method in Bravo et al. (2006), with strips computed as in Alamo et al. (2005). Generator reduction is applied after the update step using Method 4 in Yang and Scott (2018b). In addition, we denote by ZMV+F and ZFO+F the methods ZMV and ZFO with the addition of the intersection discussed in Remark 11. Since zonotopes are not closed under intersection, this intersection enclosed by converting the *a priori* enclosure X_F from CG-rep

[3] In a simplified analysis, ZMV and ZFO have computational complexities $O(n^4)$ and $O(n^5)$, respectively. See Rego et al. (2020) for a detailed discussion.

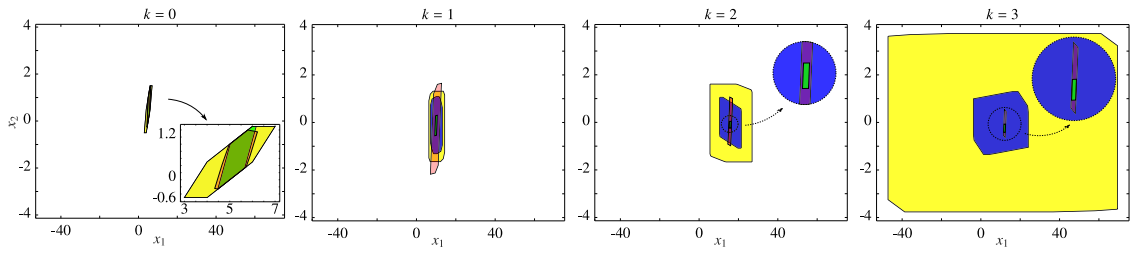

Fig. 2. The enclosures $\tilde{X}_k$ from the first four time steps of set-valued state estimation in the example in Section 5.1 using ZMV (yellow), ZFO (blue), CZMV (green), and CZFO (orange). (For interpretation of the references to color in this figure legend, the reader is referred to the web version of this article.)

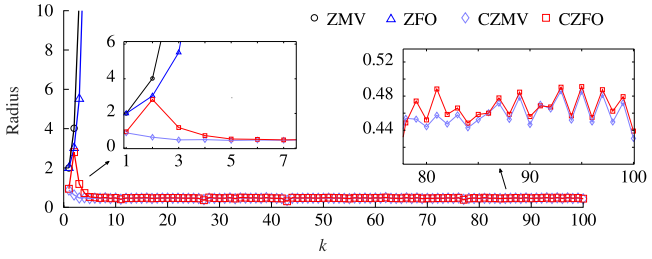

Fig. 3. The radii of the estimated enclosures $\tilde{X}_k$ in the example in Section 5.1 obtained using ZMV, ZFO, CZMV, and CZFO.

to half-space representation as described in Scott et al. (2016), representing X_F as an intersection of strips, and then using the method for bounding the intersection of a zonotope with a set of strips from Bravo et al. (2006). As with constrained zonotopes, these are referred to as ZMV-like and ZFO-like methods, respectively.

5.1. A system with nonlinear measurement equations

To demonstrate the effectiveness of our methods for set-valued state estimation of systems with nonlinear outputs, we first consider the nonlinear discrete-time system $\mathbf{x}_k = \mathbf{f}(\mathbf{x}_{k-1}) + \mathbf{w}_{k-1}$, where $\mathbf{f}$ is defined by (15) and $\mathbf{w}_k \in \mathbb{R}^2$ denotes process uncertainties with $\|\mathbf{w}_k\|_\infty \leq 0.4$. The measurements are given by

$$\begin{aligned} y_{1,k} &= x_{1,k} - \sin\left(\frac{x_{2,k}}{2}\right) + v_{1,k}, \\ y_{2,k} &= -x_{1,k}x_{2,k} + x_{2,k} + v_{2,k}, \end{aligned} \tag{17}$$

with $\|\mathbf{v}_k\|_\infty \leq 0.4$. Finally, let

$$X_0 = \left\{ \begin{bmatrix} 0.5 & 1 & -0.5 \\ 0.5 & 0.5 & 0 \end{bmatrix}, \begin{bmatrix} 5 \\ 0.5 \end{bmatrix} \right\}. \tag{18}$$

Fig. 2 shows the estimated enclosures $\tilde{X}_k$ (since there are no invariants, these are $\tilde{X}_k = \hat{X}_k$) for $k = 0, 1, 2, 3$, obtained using ZMV, ZFO, CZMV, and CZFO. In this case, Z_w and Z_v are computed as in Remark 8. The number of generators and constraints is limited to 8 and 3, respectively. The simulations were run in MATLAB 9.1 with INTLAB 12 and CPLEX 12.8, on a laptop with 32 GB RAM and an Intel Core i7-9750H processor. The first set $\tilde{X}_0$ coincides with X_0 for both ZMV and ZFO, which demonstrates that the update step method using zonotopes can be very conservative with nonlinear measurements, making the first update ineffective in this example. On the other hand, the sets $\tilde{X}_0$ obtained by CZMV and CZFO have reduced volume relative to X_0, showing that X_0 was effectively tightened by the first measurement. In addition, in contrast to CZMV and CZFO, the size of the enclosures $\tilde{X}_k$ for both ZMV and ZFO increases substantially with time. This is corroborated by Fig. 3, which illustrates the radii of the sets $\tilde{X}_k$ (half the length of the longest edge of the interval hull). Note that the radii of the sets obtained by ZMV and ZFO increase to infinity, while the radii of the sets obtained by CZMV and CZFO remain finite. This result corroborates the improved accuracy achieved by using constrained zonotopes for computing the update step with nonlinear measurement equations. Lastly, Table 2 shows the average computational times per time step of each method, together with the computational times spent in complexity reduction of the enclosures. The latter is included to distinguish the computational burden of the proposed methods from the complexity reduction procedures, whose analysis is out of the scope of this work. Note that CZMV and CZFO were able to provide accurate enclosures with an increase of 114% and 52.3% of the execution times with respect to ZMV and ZFO, respectively. Nevertheless, as mentioned above, the sets obtained by ZMV and ZFO increased to infinity in few steps, and therefore cannot provide any information about the state trajectories.

Table 2
Total and complexity reduction average execution times per time step of the state estimators for the first example.

	ZMV	CZMV	ZFO	CZFO
Total	30.5 ms	65.3 ms	47.4 ms	72.2 ms
Red.	4.4 ms	4.8 ms	6.6 ms	14.2 ms

5.2. A system with nonlinear measurements and invariants

The second example involves state estimation of the attitude of a flying robot. The robot is driven by angular velocity $\check{\mathbf{u}}_k \in \mathbb{R}^3$, with attitude expressed as a rotation quaternion $\mathbf{x}_k \in \mathbb{R}^4$ satisfying $\|\mathbf{x}_k\|_2^2 = 1$, which defines the invariant $h(\mathbf{x}_k) = \|\mathbf{x}_k\|_2^2 - 1 = 0$ to be used in the consistency step (5). The invariant $h(\mathbf{x}_k)$ is a mathematical property of rotation quaternions, which belong to the group denoted by Spin(3), where the unitary norm $\|\mathbf{x}_k\|_2^2 = 1$ is always satisfied (Selig, 2005). Therefore, even in the presence of time-varying angular velocities, disturbances and sensor noise, this invariant is satisfied by $\mathbf{x}_k$ for all $k \geq 0$.

The known value $\mathbf{u}_k$ of the physical input $\check{\mathbf{u}}_k$ is measured by gyroscopes and therefore is considered to be corrupted by additive noise $\mathbf{w}_k \in \mathbb{R}^3$. Physically, the system is driven by the uncorrupted signal $\check{\mathbf{u}}_k = \mathbf{u}_k - \mathbf{w}_k$. The attitude $\mathbf{x}_k$ evolves in discrete time according to (Lefferts et al., 1982; Teixeira et al., 2009)

$$\mathbf{x}_k = \left(\cos(p(\mathbf{u}_k, \mathbf{w}_k))\mathbf{I}_4 - \frac{T_s}{2} \frac{\sin(p(\mathbf{u}_k, \mathbf{w}_k))}{p(\mathbf{u}_k, \mathbf{w}_k)} \Omega(\mathbf{u}_k, \mathbf{w}_k) \right) \mathbf{x}_{k-1}, \tag{19}$$

where T_s is the sampling time and

$$p(\mathbf{u}_k, \mathbf{w}_k) = \frac{T_s}{2}\|\check{\mathbf{u}}_k\|_2, \quad \Omega(\mathbf{u}_k, \mathbf{w}_k) = \begin{bmatrix} 0 & \check{u}_{3,k} & -\check{u}_{2,k} & \check{u}_{1,k} \\ -\check{u}_{3,k} & 0 & \check{u}_{1,k} & \check{u}_{2,k} \\ \check{u}_{2,k} & -\check{u}_{1,k} & 0 & \check{u}_{3,k} \\ -\check{u}_{1,k} & -\check{u}_{2,k} & -\check{u}_{3,k} & 0 \end{bmatrix},$$

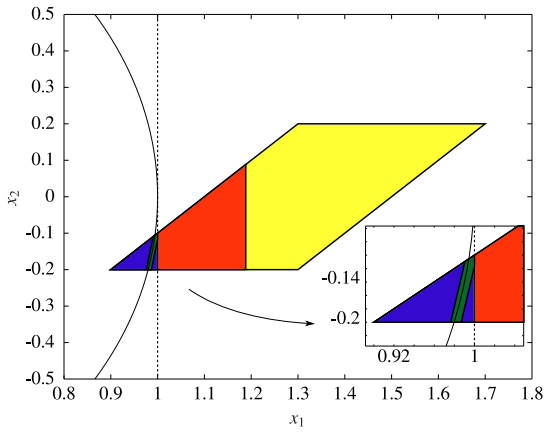

Fig. 4. The zonotope X_0 (yellow), the enclosure $\tilde{X}_0$ obtained in the consistency step (5) using Corollary 1 with $\hat{X}_0 = X_0$ (red), the set $X_0 \cap \{\mathbf{I}_2, \mathbf{0}\}$ (blue), and the enclosure $\tilde{X}_0$ obtained in the consistency step (5) using Corollary 1 with $\hat{X}_0 = X_0 \cap \{\mathbf{I}_2, \mathbf{0}\}$ (green). The resulting enclosures contain each other according to the sequence above. The dashed line denotes the box $\{\mathbf{I}_2, \mathbf{0}\}$. The circle that describes the feasible state set of $\|\mathbf{x}_0\|_2^2 = 1$ is also depicted. (For interpretation of the references to color in this figure legend, the reader is referred to the web version of this article.)

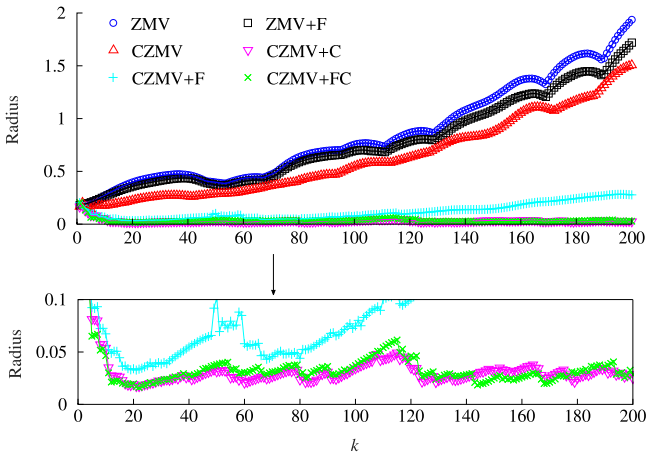

Fig. 5. The radii of the estimated enclosures $\tilde{X}_k$ for (19) obtained using ZMV-like and CZMV-like methods.

The known value $\mathbf{u}_k$ is

$$\mathbf{u}_k = \check{\mathbf{u}}_k + \mathbf{w}_k = \begin{bmatrix} 0.3\sin((2\pi/12)kT_s) \\ 0.3\sin((2\pi/12)kT_s - 6) \\ 0.3\sin((2\pi/12)kT_s - 12) \end{bmatrix} + \mathbf{w}_k, \tag{20}$$

with $\|\mathbf{w}_k\|_\infty \leq 3.0\times10^{-3}$. The measurement is given by $\mathbf{y}_k = (\mathbf{C}(\mathbf{x}_k)\mathbf{r}^{[1]}, \mathbf{C}(\mathbf{x}_k)\mathbf{r}^{[2]}) + \mathbf{v}_k$, with $\mathbf{r}^{[1]} = [1\ 0\ 0]^T$, $\mathbf{r}^{[2]} = [0\ 1\ 0]^T$, $\|\mathbf{v}_k\|_\infty \leq 0.15$, and $\mathbf{C}(\mathbf{x}_k)$ is a rotation matrix defined by

$$\mathbf{C}(\mathbf{x}_k) \triangleq \begin{bmatrix} x_{1,k}^2 - x_{2,k}^2 - x_{3,k}^2 + x_{4,k}^2 & 2(x_{1,k}x_{2,k} + x_{3,k}x_{4,k}) & 2(x_{1,k}x_{3,k} - x_{2,k}x_{4,k}) \\ 2(x_{1,k}x_{2,k} - x_{3,k}x_{4,k}) & -x_{1,k}^2 + x_{2,k}^2 - x_{3,k}^2 + x_{4,k}^2 & 2(x_{1,k}x_{4,k} + x_{2,k}x_{3,k}) \\ 2(x_{1,k}x_{3,k} + x_{2,k}x_{4,k}) & 2(-x_{1,k}x_{4,k} + x_{2,k}x_{3,k}) & -x_{1,k}^2 - x_{2,k}^2 + x_{3,k}^2 + x_{4,k}^2 \end{bmatrix}.$$

The sampling time is $T_s = 0.2$ s, and the initial state belongs to the zonotope $X_0 = \{0.18\mathbf{I}_4, [0\ 1\ 0\ 0]^T\}$. For the purpose of generating trajectories of (19), the initial state is $\mathbf{x}_0 = [0\ 1\ 0\ 0]^T$.

In the following, for the sake of clarity we first illustrate the observation described in Remark 11 for the consistency step in a sub-example with $\mathbf{x}_k \in \mathbb{R}^2$, $\|\mathbf{x}_k\|_2^2 = 1$, and

$$X_0 = \left\{ \begin{bmatrix} 0.2 & 0.2 \\ 0 & 0.2 \end{bmatrix}, \begin{bmatrix} 1.3 \\ 0 \end{bmatrix} \right\}.$$

Note that in this case the set $\{\mathbf{I}_2, \mathbf{0}\}$ is a valid enclosure for the feasible state set of the invariant $\|\mathbf{x}_k\|_2^2 = 1$. Fig. 4 shows the initial set X_0 and the enclosure $\tilde{X}_0$ obtained using Corollary 1 for the consistency step with $\hat{X}_0 = X_0$. Note that, although tightened, the resulting set is still very conservative. Fig. 4 also shows the intersection $X_0 \cap \{\mathbf{I}_2, \mathbf{0}\}$, which is tighter than the previous result. Finally, we illustrate the enclosure $\tilde{X}_0$ obtained using Corollary 1 with $\hat{X}_0 = X_0 \cap \{\mathbf{I}_2, \mathbf{0}\}$, which is the least conservative result. This demonstrates the improved accuracy that can be achieved if an enclosure of the feasible state set is known *a priori*.

Fig. 5 illustrates the radii of the enclosures $\tilde{X}_k$ obtained for the trajectories of the system (19) using ZMV-like and CZMV-like methods. We consider the enclosure $\{\mathbf{I}_4, \mathbf{0}\}$ of the feasible state set of the invariant $\|\mathbf{x}_k\|_2^2 = 1$. In this case, Z_w and Z_v are computed as in Remarks 4 and 8, respectively. The number of generators and constraints is limited to 12 and 5, respectively. Note that the zonotope methods were not able to provide useful enclosures for (19), i.e., the sizes of the enclosures increase with time and do not provide useful information, even when considering the intersection with $\{\mathbf{I}_4, \mathbf{0}\}$. Note that the enclosures provided by CZMV and CZMV+F also are not useful in this case, even though CZMV+F is much tighter than the others. On the other hand, CZMV+C and CZMV+FC both provided good enclosures with stable size, with the latter providing more accurate sets in the initial time steps, as expected. This demonstrates the advantage of including the consistency step (5) in state estimation using the mean value extension to take into account the invariant $\|\mathbf{x}_k\|_2^2 = 1$. In addition, note that the radii of the enclosures provided by CZMV+C and CZMV+FC are much smaller than the radius of $\{\mathbf{I}_4, \mathbf{0}\}$, showing that significant accuracy can be obtained by combining the state estimation procedure with the invariant, in comparison with using only the information available about the feasible state set.

Fig. 6 shows the radii of the enclosures $\tilde{X}_k$ obtained for the trajectories of (19) using ZFO-like and CZFO-like methods. Once again, the enclosures computed by zonotopes do not provide useful information since these increase with time, even when considering the intersection with $\{\mathbf{I}_4, \mathbf{0}\}$. On the other hand, even CZFO provides tight enclosures for this example. This demonstrates that the first-order Taylor extension is able to provide significantly less conservative bounds than the mean value extension in this case, since the nonlinear measurements are polynomials of second order, and therefore the interval matrices $\mathbf{Q}^{[q]}$ in Proposition 4 are singletons. Nevertheless, CZFO+C and CZFO+FC both provide still sharper enclosures, with comparable sizes due to the limited complexity of the sets. To provide a comprehensive comparison between all of the methods, Table 3 shows the average radius ratio for this example (ARR, i.e., the ratio of the radius of the set provided by one method over the radius of the set provided by another method at k, averaged over all time steps), and Table 4 shows the average computational times per time step of each method. Note that, in contrast to the analogous state estimation algorithms for linear measurements in Rego et al. (2020), the computational times of CZMV-like methods were competitive with ZMV-like methods, and CZFO-like methods with ZFO-like methods as well. The increased times of the zonotope methods arise from the iterative computation of strips based on interval analysis in Alamo et al. (2005) and the intersection with strips given in Bravo et al. (2006) to perform the update step. In this sense, using the mean value extension with constrained zonotopes, one can achieve about 93% less conservative bounds

Table 3

Average radius ratio of the enclosures obtained by the state estimators (column per row) for the system (19).

\	ZMV	ZMV+F	CZMV	CZMV+C	CZMV+F	CZMV+FC	ZFO	ZFO+F	CZFO	CZFO+C	CZFO+F	CZFO+FC
ZMV	1	0.9187	0.7193	0.0636	0.1491	0.0669	0.6447	0.6057	0.0489	0.0358	0.0436	0.0385
ZMV+F	1.0891	1	0.7834	0.0671	0.1606	0.0707	0.6988	0.6562	0.0521	0.0379	0.0465	0.0408
CZMV	1.4091	1.2946	1	0.0857	0.2024	0.0901	0.9272	0.8701	0.0680	0.0484	0.0593	0.0523
CZMV+C	29.2088	26.5557	21.4655	1	3.8897	1.0665	16.3264	15.2013	0.8974	0.6056	0.8472	0.6363
CZMV+F	8.0755	7.4009	5.6895	0.3745	1	0.4023	5.2585	4.9195	0.3382	0.2289	0.2919	0.2460
CZMV+FC	28.7622	26.1185	21.1725	0.9697	3.8402	1	15.8969	14.7785	0.8571	0.5744	0.8144	0.6018
ZFO	1.6829	1.5384	1.2325	0.0849	0.2420	0.0898	1	0.9367	0.0671	0.0487	0.0621	0.0519
ZFO+F	1.8040	1.6484	1.3211	0.0891	0.2581	0.0942	1.0683	1	0.0709	0.0512	0.0656	0.0546
CZFO	34.1796	31.0484	25.3451	1.1983	4.6785	1.2562	18.5748	17.2934	1	0.6964	0.9717	0.7290
CZFO+C	50.4008	45.7732	37.1612	1.7337	6.8068	1.8039	27.7376	25.7968	1.4945	1	1.4372	1.0499
CZFO+F	33.4713	30.4709	24.4434	1.2814	4.5068	1.3433	19.2573	17.9445	1.1000	0.7504	1	0.7929
CZFO+FC	50.2958	45.6286	37.2526	1.6647	6.8396	1.7317	27.1388	25.2164	1.4323	0.9617	1.3947	1

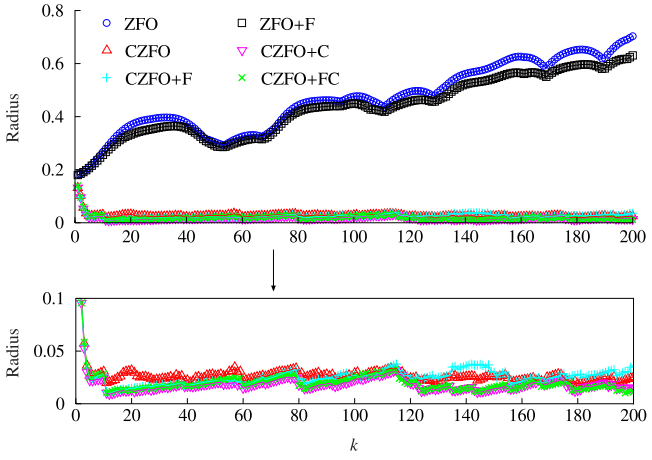

Fig. 6. The radii of the estimated enclosures $\tilde{X}_k$ for (19) obtained using ZFO-like and CZFO-like methods.

(CZMV+C–to–ZMV+F ARR of only 6.7%) in comparison to zonotopes, with a mild increase of 22.2% in the average execution time. On the other hand, using the first-order Taylor extension, one can achieve about 95% less conservative bounds (CZFO+C–to–ZFO+F ARR of 5.1%), with an increase of 10.5% in the average execution time. This demonstrates the joint accuracy and efficiency provided by the proposed methods based on constrained zonotopes. These ARR are highlighted in Table 3, and correspond to a comparison between the most accurate results obtained by ZMV-like and CZMV-like methods, and between ZFO-like and CZFO-like methods.

Lastly, note that the CZFO+C–to–CZFO ARR was of 69.64%, showing again the improved accuracy obtained by taking into account the invariant through the consistency step. In addition, CZFO-like methods provided better enclosures than CZMV-like methods in this example. Nevertheless, this comes with an important increase in computational time as shown in Table 4. This demonstrates that the choice between CZMV-like methods and CZFO-like methods for state estimation can provide a trade-off between accuracy and efficiency, and therefore will depend on the current application.

Remark 15. Although the examples in this section are low-dimensional, the proposed methods can be applied straightforwardly to higher dimensional systems, such as the quaternion-based quadrotor model in Kang et al. (2020). The computational complexity will follow the expressions shown in Table 1.

Table 4
Total and complexity reduction average execution times per time step of the state estimators for the system (19).

	ZMV	ZMV+F	CZMV	CZMV+C	CZMV+F	CZMV+FC
Total	0.4552 s	0.4610 s	0.4478 s	0.5635 s	0.4519 s	0.5942 s
Red.	0.37 ms	0.31 ms	10.6 ms	71.8 ms	19.8 ms	96.5 ms
	ZFO	ZFO+F	CZFO	CZFO+C	CZFO+F	CZFO+FC
Total	1.0403 s	1.0563 s	1.0907 s	1.1671 s	1.1009 s	1.3750 s
Red.	2.3 ms	2.2 ms	90.3 ms	0.1266 s	98.7 ms	0.3306 s

6. Conclusions

This paper developed new approaches for set-valued state estimation of nonlinear discrete-time systems with nonlinear measurements and nonlinear invariants. The state trajectories were enclosed using the standard prediction-update algorithm with the addition of a new consistency step accounting for the nonlinear invariants. New methods were proposed for the update and consistency steps using generalized intersections of constrained zonotopes. In addition, our previous methods for the prediction step were generalized to allow the approximation points for the mean value and first-order Taylor extensions to lie in a larger region. Numerical results demonstrate that our methods can provide significantly tighter enclosures compared to existing zonotope methods. The improved accuracy is achieved with a mild increase in computational cost. Nevertheless, future work will seek to reduce the execution times, since these can be a major issue in many practical applications, and to reduce the conservativeness introduced by the mean value and first-order Taylor approximations.

Acknowledgments

This work has been (partially) supported by the Italian Ministry for Research, Italy in the framework of the 2017 Program for Research Projects of National Interest (PRIN), Grant no. 2017YKXYXJ, the project INCT under the grant CNPq, Brazil 465755/2014-3, FAPESP, Brazil 2014/50851-0, and also by the agencies CAPES, Brazil under the grants 001 and 88887.136349/2017-00, and FAPEMIG, Brazil. This material is also based upon work supported by the National Science Foundation, USA under grant no. 1949748.

Appendix A. Proofs

Proof of Proposition 1. Choose any $(\mathbf{x}, \mathbf{w}) \in X \times W$. Lemma 1 ensures that there exists a real matrix $\hat{\mathbf{J}} \in \mathbf{J}$ such that $\mathbf{f}(\mathbf{x}, \mathbf{u}, \mathbf{w}) = \mathbf{f}(\boldsymbol{\gamma}_x, \mathbf{u}, \mathbf{w}) + \hat{\mathbf{J}}(\mathbf{x} - \boldsymbol{\gamma}_x)$. By Theorem 1 and the choice of Z_w, it follows that $\mathbf{f}(\mathbf{x}, \mathbf{u}, \mathbf{w}) \in Z_w \oplus \triangleleft\left(\mathbf{J}, X - \boldsymbol{\gamma}_x\right)$, as desired. ■

Proof of Proposition 2. Choose any $(\mathbf{x}, \mathbf{w}) = \mathbf{z} \in Z$. Lemma 2 ensures that there exist $\boldsymbol{\xi} \in B_\infty(\mathbf{A}, \mathbf{b})$, $\tilde{\boldsymbol{\xi}} \in B_\infty(\tilde{\mathbf{A}}, \tilde{\mathbf{b}})$, and $\hat{\mathbf{L}} \in \mathbf{L}$, such that

$$\begin{aligned}\mathbf{f}(\mathbf{x}, \mathbf{u}, \mathbf{w}) = \mathbf{f}(\boldsymbol{\gamma}_x, \mathbf{u}, \boldsymbol{\gamma}_w) + \nabla^T \mathbf{f}(\boldsymbol{\gamma}_x, \mathbf{u}, \boldsymbol{\gamma}_w)(\mathbf{z} - \boldsymbol{\gamma}_z) \\ + \tilde{\mathbf{c}} + [\tilde{\mathbf{G}} \ \tilde{\mathbf{G}}_\mathbf{d}]\tilde{\boldsymbol{\xi}} + \hat{\mathbf{L}}((\mathbf{c} - \boldsymbol{\gamma}_z) + 2\mathbf{G}\boldsymbol{\xi}).\end{aligned}$$

Therefore, $\mathbf{f}(\mathbf{x}, \mathbf{u}, \mathbf{w}) \in \mathbf{f}(\boldsymbol{\gamma}_x, \mathbf{u}, \boldsymbol{\gamma}_w) \oplus \nabla^T \mathbf{f}(\boldsymbol{\gamma}_x, \mathbf{u}, \boldsymbol{\gamma}_w)(Z - \boldsymbol{\gamma}_z) \oplus \triangleleft(\mathbf{L}, (\mathbf{c} - \boldsymbol{\gamma}_z) \oplus 2\mathbf{G}B_\infty(\mathbf{A}, \mathbf{b})) \oplus \tilde{\mathbf{c}} \oplus [\tilde{\mathbf{G}} \ \tilde{\mathbf{G}}_\mathbf{d}]B_\infty(\tilde{\mathbf{A}}, \tilde{\mathbf{b}})$. Thus, (14) follows immediately from the definition of R. ■

Proof of Proposition 5. Each component of $(\mathbf{J} - \text{mid}(\mathbf{J})) \in \mathbb{IR}^{m \times n}$ is an interval satisfying $(J_{ij} - \text{mid}(J_{ij})) = (1/2)\text{diam}(J_{ij})[-1, 1]$. Moreover, $a[-1, 1] = |a|[-1, 1]$ holds for every $a \in \mathbb{R}$. Therefore $m_{\boldsymbol{\gamma},i} = \sum_{j=1}^{n} (1/2)\text{diam}(J_{ij})|\bar{c}_{\boldsymbol{\gamma},j}|[-1, 1]$. Consequently, $\text{diam}(m_{\boldsymbol{\gamma},i}) \sum_{j=1}^{n} \text{diam}(J_{ij})|\bar{c}_{\boldsymbol{\gamma},j}|$, and

$$\begin{aligned}\|\text{diam}(\mathbf{m}_\gamma)\|_1 &= \sum_{i=1}^{m}\sum_{j=1}^{n} \text{diam}(J_{ij})|\bar{c}_{\boldsymbol{\gamma},j}| = \sum_{j=1}^{n}\left(\sum_{i=1}^{m} \text{diam}(J_{ij})\right)|\bar{c}_{\boldsymbol{\gamma},j}| \\ &= \sum_{j=1}^{n} \Theta_{jj}|\bar{c}_{\boldsymbol{\gamma},j}| = \|\boldsymbol{\Theta}\bar{\mathbf{c}}_\gamma\|_1.\end{aligned}$$

The constraints in (16) follow directly from the requirement that $\boldsymbol{\gamma} \in \square Z$. ■

Proof of Corollary 1. Choose any $\mathbf{x} \in X$ satisfying $\mathbf{h}(\mathbf{x}) = \mathbf{0}$. Lemma 1 ensures that there exists a real matrix $\hat{\mathbf{J}} \in \mathbf{J}$ such that $\mathbf{h}(\mathbf{x}) = \mathbf{h}(\boldsymbol{\gamma}_x) + \hat{\mathbf{J}}(\mathbf{x} - \boldsymbol{\gamma}_x)$. Since $\tilde{\mathbf{J}} = \tilde{\mathbf{J}} + (\hat{\mathbf{J}} - \tilde{\mathbf{J}})$ holds, then $\mathbf{h}(\mathbf{x}) = \mathbf{h}(\boldsymbol{\gamma}_x) + \tilde{\mathbf{J}}(\mathbf{x} - \boldsymbol{\gamma}_x) + (\hat{\mathbf{J}} - \tilde{\mathbf{J}})(\mathbf{x} - \boldsymbol{\gamma}_x)$. Consequently,

$$\begin{aligned}\tilde{\mathbf{J}}\mathbf{x} &= \mathbf{h}(\mathbf{x}) + \tilde{\mathbf{J}}\boldsymbol{\gamma}_x - \mathbf{h}(\boldsymbol{\gamma}_x) + (\tilde{\mathbf{J}} - \hat{\mathbf{J}})(\mathbf{x} - \boldsymbol{\gamma}_x) \\ &= \mathbf{0} + \tilde{\mathbf{J}}\boldsymbol{\gamma}_x - \mathbf{h}(\boldsymbol{\gamma}_x) + (\tilde{\mathbf{J}} - \hat{\mathbf{J}})(\mathbf{x} - \boldsymbol{\gamma}_x) \\ &\in (\tilde{\mathbf{J}}\boldsymbol{\gamma}_x - \mathbf{h}(\boldsymbol{\gamma}_x)) \oplus \triangleleft(\tilde{\mathbf{J}} - \mathbf{J}, X - \boldsymbol{\gamma}_x) = H.\end{aligned}$$

Therefore, $\{\mathbf{x} \in X : \mathbf{h}(\mathbf{x}) = \mathbf{0}\} \subseteq \{\mathbf{x} \in X : \tilde{\mathbf{J}}\mathbf{x} \in H\} = X \cap_\mathbf{D} H$. ■

Proof of Corollary 2. Choose $\mathbf{x} \in X$ such that $\mathbf{h}(\mathbf{x}) = \mathbf{0}$. Lemma 2 ensures that there exist $\boldsymbol{\xi} \in B_\infty(\mathbf{A}, \mathbf{b})$, $\tilde{\boldsymbol{\xi}} \in B_\infty(\tilde{\mathbf{A}}, \tilde{\mathbf{b}})$, and $\hat{\mathbf{L}} \in \mathbf{L}$, such that

$$\begin{aligned}\mathbf{h}(\mathbf{x}) = \mathbf{h}(\boldsymbol{\gamma}_x) + \nabla_x^T \mathbf{h}(\boldsymbol{\gamma}_x)(\mathbf{x} - \boldsymbol{\gamma}_x) \\ + \hat{\mathbf{L}}(\mathbf{p} + 2\mathbf{G}\boldsymbol{\xi}) + \tilde{\mathbf{c}} + [\tilde{\mathbf{G}} \ \tilde{\mathbf{G}}_\mathbf{v}]\tilde{\boldsymbol{\xi}}.\end{aligned}$$

with $\mathbf{p} = \mathbf{c} - \boldsymbol{\gamma}_x$. Since $\mathbf{h}(\mathbf{x}) = \mathbf{0}$, we have $\nabla_x^T \mathbf{h}(\boldsymbol{\gamma})\mathbf{x} = -\mathbf{h}(\boldsymbol{\gamma}_x) + \nabla_x^T \mathbf{h}(\boldsymbol{\gamma}_x)\boldsymbol{\gamma}_x - \hat{\mathbf{L}}(\mathbf{p} + 2\mathbf{G}\boldsymbol{\xi}) - \tilde{\mathbf{c}} - [\tilde{\mathbf{G}} \ \tilde{\mathbf{G}}_\mathbf{v}]\tilde{\boldsymbol{\xi}}$, and therefore

$$\nabla_x^T \mathbf{h}(\boldsymbol{\gamma}_x)\mathbf{x} \in (-\mathbf{h}(\boldsymbol{\gamma}_x) + \nabla_x^T \mathbf{h}(\boldsymbol{\gamma}_x)\boldsymbol{\gamma}_x) \oplus (-R) = H.$$

We conclude that $\{\mathbf{x} \in X : \mathbf{h}(\mathbf{x}) = \mathbf{0}\} \subseteq \{\mathbf{x} \in X : \nabla_x^T \mathbf{h}(\boldsymbol{\gamma}_x)\mathbf{x} \in H\} = X \cap_\mathbf{D} H$. ■

Appendix B. Linear systems

When the prediction, update, and consistency steps for nonlinear systems developed in the previous subsections are applied directly to linear systems, the resulting enclosures are straightforward. Consider the linear discrete-time system

$$\mathbf{x}_k = \mathbf{A}\mathbf{x}_{k-1} + \mathbf{B}_u\mathbf{u}_{k-1} + \mathbf{B}_w\mathbf{w}_{k-1}, \tag{B.1a}$$

$$\mathbf{y}_k = \mathbf{C}\mathbf{x}_k + \mathbf{D}_u\mathbf{u}_k + \mathbf{D}_v\mathbf{v}_k, \tag{B.1b}$$

where $\mathbf{A} \in \mathbb{R}^{n \times n}$, $\mathbf{B}_u \in \mathbb{R}^{n \times n_u}$, $\mathbf{B}_w \in \mathbb{R}^{n \times n_w}$, $\mathbf{C} \in \mathbb{R}^{n_y \times n}$, $\mathbf{D}_u \in \mathbb{R}^{n_y \times n_u}$, $\mathbf{D}_v \in \mathbb{R}^{n_y \times n_v}$, with known polytopic bounds $(\mathbf{x}_0, \mathbf{w}_k, \mathbf{v}_k) \in X_0 \times W \times V$. Moreover, assume that the trajectories of (B.1) satisfy the linear invariants $\mathbf{E}\mathbf{x}_k = \mathbf{d}$, with $\mathbf{E} \in \mathbb{R}^{n_\mathbf{d} \times n}$, and $\mathbf{d} \in \mathbb{R}^{n_\mathbf{d}}$. Given the previous set $\tilde{X}_{k-1}$, the prediction step (3) and the update step (4) are computed exactly for (B.1a)–(B.1b) as in Scott et al. (2016):

$$\bar{X}_k = \mathbf{A}\tilde{X}_{k-1} \oplus \mathbf{B}_u\mathbf{u}_{k-1} \oplus \mathbf{B}_w W, \tag{B.2}$$

$$\hat{X}_k = \bar{X}_k \cap_\mathbf{C} ((\mathbf{y}_k - \mathbf{D}_u\mathbf{u}_k) \oplus (-\mathbf{D}_v V)). \tag{B.3}$$

All the set operations in (B.2)–(B.3) can be computed straightforwardly using (10)–(12). To compute the consistency step (5), note that in this case this can be written as $\tilde{X}_k \supseteq \{\mathbf{x} \in \hat{X}_k : \mathbf{E}\mathbf{x}_k \in \{\mathbf{d}\}\}$, where $\{\mathbf{d}\}$ denotes a singleton that contains only the point $\mathbf{d}$. Therefore, if $\hat{X}_k = \{\hat{\mathbf{G}}_k, \hat{\mathbf{c}}_k, \hat{\mathbf{A}}_k, \hat{\mathbf{b}}_k\}$, then $\tilde{X}_k$ is given by

$$\tilde{X}_k = \hat{X}_k \cap_\mathbf{E} \{\mathbf{d}\} = \left\{\hat{\mathbf{G}}_k, \hat{\mathbf{c}}_k, \begin{bmatrix}\hat{\mathbf{A}}_k \\ \mathbf{E}\hat{\mathbf{G}}_k\end{bmatrix}, \begin{bmatrix}\hat{\mathbf{b}}_k \\ \mathbf{d} - \mathbf{E}\hat{\mathbf{c}}_k\end{bmatrix}\right\}. \tag{B.4}$$

Hence, the consistency step can be computed exactly as well. Therefore, the only source of conservatism in the set-valued state estimation of (B.1) using constrained zonotopes through the steps (B.2)–(B.4) arises if the complexity of the sets are limited, which is often necessary in practice and requires the use of complexity reduction methods (Scott et al., 2016).

References

Alamo, T., Bravo, J., & Camacho, E. (2005). Guaranteed state estimation by zonotopes. *Automatica*, *41*(6), 1035–1043.

Alamo, T., Bravo, J. M., Redondo, M. J., & Camacho, E. F. (2008). A set-membership state estimation algorithm based on DC programming. *Automatica*, *44*(1), 216–224.

Bravo, J. M., Alamo, T., & Camacho, E. F. (2006). Bounded error identification of systems with time-varying parameters. *IEEE Transactions on Automatic Control*, *51*(7), 1144–1150.

Chabane, S. B., Maniu, C. S., Alamo, T., Camacho, E., & Dumur, D. (2014). Improved Set-Membership Estimation Approach based on Zonotopes and Ellipsoids. In *Proc. of the 2014 European Control Conference* (pp. 993–998).

Chabert, G., & Jaulin, L. (2009). Contractor programming. *Artificial Intelligence*, *173*, 1079–1100.

Chisci, L., Garulli, A., & Zappa, G. (1996). Recursive state bounding by parallelotopes. *Automatica*, *32*(7), 1049–1055.

Combastel, C. (2005). A state bounding observer for uncertain non-linear continuous-time systems based on zonotopes. In *Proc. of the 44th IEEE Conference on Decision and Control, and 2005 European Control Conference* (pp. 7228–7234).

Combastel, C. (2015). Merging Kalman Filtering and Zonotopic State Bounding for Robust Fault Detection under Noisy Environment. In *Proc. of the 9th IFAC Symposium on Fault Detection, Supervision and Safety for Technical Processes* (pp. 289–295).

Durieu, C., Walter, E., & Polyak, B. (2001). Multi-input multi-output ellipsoidal state bounding. *Journal of Optimization Theory and Applications*, *111*(2), 273–303.

Eras-Herrera, W. Y., Mesquita, A. R., & Teixeira, B. O. S. (2019). Equality-constrained state estimation for hybrid systems. *IET Control Theory & Applications*, *13*(13), 2018–2028.

Girard, A., & Guernic, C. L. (2008). Efficient Reachability Analysis for Linear Systems using Support Functions. In *Proc. of the 17th IFAC World Congress* (pp. 8966–8971).

Goodarzi, F. A., & Lee, T. (2017). Global formulation of an extended Kalman filter on SE(3) for geometric control of a quadrotor UAV. *Journal of Intelligent and Robotic Systems*, *88*(2), 395–413.

Jaulin, L. (2009). Robust set-membership state estimation; application to underwater robotics. *Automatica*, *45*(1), 202–206.

Jaulin, L. (2016). Inner and outer set-membership state estimation. *Reliable Computing*, *22*, 47–55.

Julier, S. J., & LaViola, J. J. (2010). On Kalman filtering with nonlinear equality constraints. *IEEE Transactions on Signal Processing*, *55*(6), 2774–2784.

Kang, J.-W., Sadegh, N., & Urschel, C. (2020). Quaternion Based Nonlinear Trajectory Control of Quadrotors with Guaranteed Stability. In *Proc. of the 2020 IEEE American Control Conference* (pp. 3834–3839).

Kelner, J. A., & Spielman, D. A. (2006). A randomized polynomial-time simplex algorithm for linear programming. In *Proc. of the 38th Annual ACM Symposium on Theory of Computing* (pp. 51–60).

Kochdumper, N., & Althoff, M. (2020). Reachability analysis for hybrid systems with nonlinear guard sets. In *Proc. of the 23rd International Conference on Hybrid Systems: Computation and Control* (pp. 1–10).

Kühn, W. (1998). Rigorously computed orbits of dynamical systems without the wrapping effect. *Computing*, *61*(1), 47–67.

Le, V. T. H., Stoica, C., Alamo, T., Camacho, E. F., & Dumur, D. (2013). Zonotopic guaranteed state estimation for uncertain systems. *Automatica*, *49*(11), 3418–3424.

Lefferts, E. J., Markley, F. L., & Shuster, M. D. (1982). Kalman filtering for spacecraft attitude estimation. *Journal of Guidance, Control, and Dynamics*, *5*(5), 417–429.

Moore, R. E., Kearfott, R. B., & Cloud, M. J. (2009). *Introduction to Interval Analysis*. Philadelphia, PA, USA: SIAM.

Platzer, A., & Clarke, E. M. (2007). The Image Computation Problem in Hybrid Systems Model Checking. In *Proc. of the International Workshop on Hybrid Systems: Computation and Control* (pp. 473–486).

Polyak, B. T., Nazin, S. A., Durieu, C., & Walter, E. (2004). Ellipsoidal parameter or state estimation under model uncertainty. *Automatica*, *40*(7), 1171–1179.

Raimondo, D. M., Marseglia, G. R., Braatz, R. D., & Scott, J. K. (2016). Closed-loop input design for guaranteed fault diagnosis using set-valued observers. *Automatica*, *74*, 107–117.

Rego, B. S., & Raffo, G. V. (2019). Suspended load path tracking control using a tilt-rotor UAV based on zonotopic state estimation. *Journal of the Franklin Institute*, *356*(4), 1695–1729.

Rego, B. S., Raffo, G. V., Scott, J. K., & Raimondo, D. M. (2020). Guaranteed methods based on constrained zonotopes for set-valued state estimation of nonlinear discrete-time systems. *Automatica*, *111*, Article 108614.

Rego, B. S., Raimondo, D. M., & Raffo, G. V. (2018a). Path Tracking Control with State Estimation based on Constrained Zonotopes for Aerial Load Transportation. In *Proc. of the 57th IEEE Conference on Decision and Control* (pp. 1979–1984).

Rego, B. S., Raimondo, D. M., & Raffo, G. V. (2018b). Set-based state estimation of nonlinear systems using constrained zonotopes and interval arithmetic. In *Proc. of the 2018 European Control Conference* (pp. 1584–1589).

Rotella, N., Bloesch, M., Righetti, L., & Schaal, S. (2014). State Estimation for a Humanoid Robot. In *Proc. of the 2014 IEEE/RSJ International Conference Intelligent Robots and Systems* (pp. 952–958).

Saeedi, S., Trentini, M., Seto, M., & Li, H. (2016). Multiple-robot simultaneous localization and mapping: A review. *Journal of Field Robotics*, *33*(1), 3–46.

Schweppe, F. (1968). Recursive state estimation: Unknown but bounded errors and system inputs. *IEEE Transactions on Automatic Control*, *13*(1), 22–28.

Scott, J. K., Marseglia, G. R., Magni, L., Braatz, R. D., & Raimondo, D. M. (2013). A Hybrid Stochastic-Deterministic Input Design Method for Active Fault Diagnosis. In *Proc. of the 52nd IEEE Conference on Decision and Control* (pp. 5656–5661).

Scott, J. K., Raimondo, D. M., Marseglia, G. R., & Braatz, R. D. (2016). Constrained zonotopes: a new tool for set-based estimation and fault detection. *Automatica*, *69*, 126–136.

Selig, J. M. (2005). *Geometric Fundamentals of Robotics* (2nd ed.). Springer.

Shamma, J. S., & Tu, K.-Y. (1997). Approximate set-valued observers for nonlinear systems. *IEEE Transactions on Automatic Control*, *42*(5), 648–658.

Shen, K., & Scott, J. K. (2017). Rapid and accurate reachability analysis for nonlinear dynamic systems by exploiting model redundancy. *Computers & Chemical Engineering*, *106*, 596–608.

Simon, D. (2006). *Optimal State Estimation: Kalman, H_∞ and Nonlinear Approaches*. John Wiley & Sons, Inc.

Simon, D. (2010). Kalman filtering with state constraints: a survey of linear and nonlinear algorithms. *IET Control Theory & Applications*, *4*(8), 1303–1318.

Teixeira, B. O. S., Chandrasekar, J., Tôrres, L. A. B., Aguirre, L. A., & Bernstein, D. S. (2009). State estimation for linear and non-linear equality-constrained systems. *International Journal of Control*, *82*(5), 918–936.

Yang, C., & Blash, E. (2009). Kalman filtering with nonlinear state constraints. *IEEE Transactions on Aerospace and Electronic Systems*, *45*(1), 70–84.

Yang, F., & Li, Y. (2009). Set-membership filtering for discrete-time systems with nonlinear equality constraints. *IEEE Transactions on Automatic Control*, *54*(10), 2480–2486.

Yang, X., & Scott, J. K. (2018a). Accurate Set-Based State Estimation for Nonlinear Discrete-Time Systems using Differential Inequalities with Model Redundancy. In *Proc. of the 57th IEEE Conference on Decision and Control* (pp. 680–685).

Yang, X., & Scott, J. K. (2018b). A comparison of zonotope order reduction techniques. *Automatica*, *95*, 378–384.

Yang, X., & Scott, J. K. (2020). Accurate uncertainty propagation for discrete-time nonlinear systems using differential inequalities with model redundancy. *IEEE Transactions on Automatic Control*, *65*(12), 5043–5057.

Zhang, Y., & Jiang, J. (2008). Bibliographical review on reconfigurable fault-tolerant control systems. *Annual Reviews in Control*, *32*, 229–252.

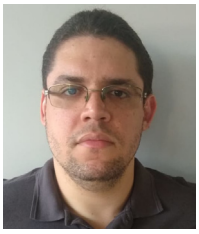

Brenner S. Rego is currently a Ph.D. candidate in Electrical Engineering at the Federal University of Minas Gerais, Brazil. He received his B.S. in Electrical Engineering from the Federal University of Goiás, in 2014, and his M.S. in Electrical Engineering from the Federal University of Minas Gerais, in 2016. He is the author or co-author of diverse papers published in refereed journals and conference proceedings. His current research interests include active fault diagnosis and fault-tolerant control, set-valued state estimation, modeling and control of unmanned aerial vehicles, and aerial load transportation.

Joseph K. Scott is an Associate Professor in the Department of Chemical and Biomolecular Engineering at the Georgia Institute of Technology. He received his B.S. (2006) in Chemical Engineering from Wayne State University, and his M.S. (2008) and Ph.D. (2012) in Chemical Engineering from MIT. His honors include the 2012 Best Paper Award from the Journal of Global Optimization, the 2016 W. David Smith, Jr. Award from the Computing and System Technology Division of the AIChE, the 2014–2016 Automatica Paper Prize from the International Federation of Automatic Control, and the 2016 Air Force Young Investigator Paper Prize from the International Federation of Automatic Control, and the 2016 Air Force Young Investigator Research Program Award. His research interests include dynamical systems, optimization theory, simulation and optimization of chemical processes, advanced process control, and fault diagnosis.

Davide M. Raimondo received the Ph.D. in Electronics, Computer Science and Electrical Engineering from the University of Pavia, Italy, in 2009. From January 2009 to December 2010 he was a postdoctoral fellow in the Automatic Control Laboratory, ETH Zurich, Switzerland. From December 2010 to May 2015 he was assistant professor at University of Pavia. He has held visiting positions at the Massachusetts Institute of Technology, University of Seville, Vienna University of Technology, University of Konstanz. Prof. Raimondo is currently an associate professor and head of the educational Process Control Lab in the Department of Electrical, Computer and Biomedical Engineering at University of Pavia, Italy. He is the author or co-author of more than 100 papers published in refereed journals, edited books, and refereed conference proceedings. He serves as subject editor for the journals Automatica and IEEE Transactions on Control Systems Technology and as CEB member of IEEE Control Systems Society. His current research interests include advanced battery management systems, setbased estimation, fault diagnosis and fault-tolerant control, model predictive control and optimization. In 2017, Prof. Raimondo, with co-authors, received the 2014–2016 Automatica Paper Prize Award.

Guilherme V. Raffo was born in Porto Alegre, Brazil. He received the B.Sc. degree in automation and control engineering from the Pontifical Catholic University of Rio Grande do Sul, Brazil, in 2002, his specialist degree in industrial automation from the Federal University of Rio Grande do Sul, Brazil, in 2003, his M.Sc. degree in electrical engineering from the Federal University of Santa Catarina, Brazil, in 2005, his M.Sc. degree in automation, robotics and telematic in 2007 and his Ph.D. degree in 2011, both from the University of Seville, Spain, and was a Postdoctoral fellow in 2011–2012 at the Federal University of Santa Catarina, Brazil. He is currently an Associate Professor at Federal University of Minas Gerais, Brazil. He is the author or coauthor of more than 90 publications including journal papers, book chapters, and conference proceedings. His current research interests include robust control, nonlinear control, H_∞ control theory, predictive control, set-membership state estimation, fault-tolerant control, unmanned aerial vehicles, robotics, and underactuated systems.